AD-A071 362 AERONAUTICAL RESEARCH LABS MELBOURNE (AUSTRALIA) F/G 20/4
THE EFFECT OF BLEED ON TWO-DIMENSIONAL BASE FLOW AT SUBSONIC, T--ETC(U)
NOV 78 N POLLOCK

UNCLASSIFIED ARL/AERO NOTE-381 NL

| OF |
AD
A071362

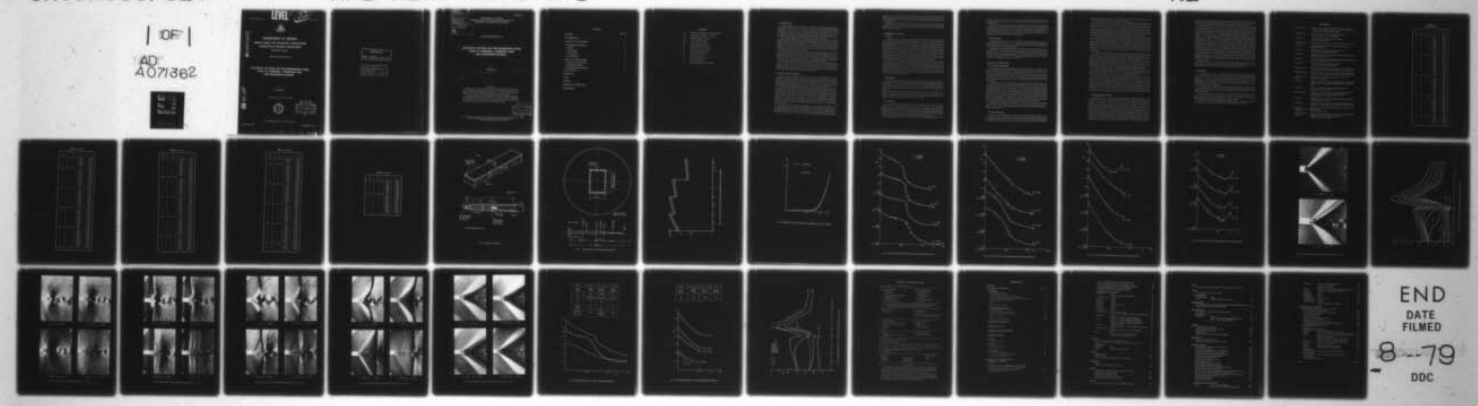

END
DATE FILMED
8-79
DDC

ARL-AERO-NOTE-381

AR-001-321

DEPARTMENT OF DEFENCE

DEFENCE SCIENCE AND TECHNOLOGY ORGANISATION

AERONAUTICAL RESEARCH LABORATORIES

MELBOURNE, VICTORIA

AERODYNAMICS NOTE 381

THE EFFECT OF BLEED ON TWO-DIMENSIONAL BASE FLOW AT SUBSONIC, TRANSONIC AND LOW SUPERSONIC SPEEDS

by

N. POLLOCK

Approved for Public Release.

COPY No 12

NOVEMBER, 1978

AR-001-321

DEPARTMENT OF DEFENCE
DEFENCE SCIENCE AND TECHNOLOGY ORGANISATION
AERONAUTICAL RESEARCH LABORATORIES

AERODYNAMICS NOTE 381

THE EFFECT OF BLEED ON TWO-DIMENSIONAL BASE FLOW AT SUBSONIC, TRANSONIC AND LOW SUPERSONIC SPEEDS

(11) Nov 78

by

(10) N. POLLOCK

(12) 39 p.

(14) ARL/AERO NOTE-381

SUMMARY

Measurements of the effect of bleed on the base pressure acting on a two-dimensional blunt trailing edge aerofoil are reported and schlieren photographs of the base flow are presented. The tests covered a Mach number range of 0·5 to 1·35 at a base height Reynolds number of approximately 9 × 10⁴ with turbulent approach boundary layers.

The results indicate that small bleed quantities can produce considerably greater base drag reductions at transonic speeds than at subsonic or supersonic speeds. A bleed mass flow coefficient of 0·07 produces a lower base drag than the best practical non-bleed blunt trailing edge geometry through the entire test Mach number range.

POSTAL ADDRESS: Chief Superintendent, Aeronautical Research Laboratories,
Box 4331, P.O., Melbourne, Victoria, 3001, Australia.

CONTENTS

NOTATION

C_{pb}	Base pressure coefficient $= (P_b - P_0)/(\gamma P_0 M_0^2/2)$
C_q	Bleed mass flow coefficient $= Q/U_0\rho_0 h$
h	Model base height (15·2 *mm*)
M_0	Free stream Mach number
P_0	Free stream static pressure.
P_b	Static pressure in plane of base.
Q	Bleed mass flow per unit span.
R_e	Reynolds number based on h.
U_0	Free stream velocity.
γ	Ratio of specific heats (1·4).
ρ_0	Free stream density.
θ	Boundary layer momentum thickness.

1. INTRODUCTION

It has been pointed out by various authors[1,2,3] that aerofoils with blunt trailing edges have many potential advantages in the transonic speed range. A number of the recently designed "supercritical" aerofoil sections[4,5] incorporate a small amount of trailing edge bluntness. At the present time the more extensive use of blunt trailing edges is prevented by the occurrence of a significant "base drag" penalty when the base height to chord ratio exceeds about 1%. Any method of reducing two dimensional subsonic and transonic base drag will permit the use of thicker blunt trailing edges with their attendant aerodynamic advantages[1,2,3].

Many geometric modifications to blunt trailing edges aimed at reducing base drag have been investigated. Overall the most promising designs appear to be the serrated or segmented trailing edges developed independently by Tanner[8] and the present author[7]. These base geometries give a drag reduction of about 60% over a simple blunt base. Greater drag reductions have been obtained[6] using thick splitter plates or wedges attached to the base, but these arrangements are not attractive for transonic aerofoils since they would exhibit many of the problems associated with conventional sharp trailing edges.

An alternative approach to the reduction of two dimensional base drag is the use of base bleed. Tests at low[9,10] and supersonic[11–14] speeds have shown that bleeding low velocity air into the base region produces a marked reduction in drag. On the basis of these results it appears highly probable that transonic base drag would also be reduced by the use of bleed. Unfortunately to the best of the author's knowledge there are no published measurements of the effect of transonic base bleed, presumably due to the experimental difficulties involved.

In this note measurements of the effect of base bleed on base pressure in the Mach number range $0{\cdot}50 \leqslant M_0 \leqslant 1{\cdot}35$ are presented. The primary aim of these tests was to determine whether base bleed could be used to produce a lower base drag than that obtained from the currently available modified trailing edge geometries. The experimental work described here was carried out in the transonic wind tunnel during June 1978.

2. NOTES ON TEST METHODS

When testing two dimensional blunt base aerofoil models in wind tunnels there is a strong tendency for the tunnel sidewall boundary layers to flow into the low pressure base region destroying the two dimensionality of the base flow. Low speed tests[15] suggest that a model aspect ratio (span/chord) exceeding 4 (for a model with a base height/chord ratio of 0·17) is required if the tunnel centreline base pressure is to be reasonably close to its two-dimensional value. Similar three dimensional flow problems are known to occur at supersonic speeds[13,16].

If a model of an acceptably large aspect ratio is used, considerable difficulty is experienced in ducting the necessary bleed air into the model and distributing it evenly over the span. This problem, which is significant at low speed[9,10] becomes prohibitively difficult at transonic and supersonic speeds. For supersonic base flows which are steady and symmetrical it is possible to use a blackward facing step in the tunnel wall rather than an aerofoil model. The bleed air ducts are then no longer subject to arbitrary size restrictions. The supersonic tests reported in References 12, 13 and 14 used rearward facing steps while the complete aerofoil tests in Reference 11 were carried out with the excessively low aspect ratios of 1·0 and 0·7. At compressible subsonic and transonic speeds, as at low speed, the base flow is unsteady and a complete aerofoil model must be used.

For the tests reported here the novel arrangement of using a hollow model with an inlet slit along the leading edge to provide the bleed flow was adopted. This technique makes it relatively simple to obtain a uniform spanwise distribution of bleed flow. The disadvantage of this method is that the flow around the model will be altered as the bleed mass flow is varied. The effect of the inlet flow can simply be considered as resulting in an effective model thickness

equal to $(1 - C_q)$ times the physical model thickness. Fortunately comparisons between earlier blunt trailing edge aerofoil tests at subsonic, transonic and supersonic speeds[17,18] suggest that the base pressure is primarily dependent on free stream Mach number and relatively insensitive to model geometry.

Both subsonic[9] and supersonic[11] tests have shown that for best results the bleed air must be introduced into the base region at as low a velocity as possible. For this reason the model designed for the present tests had an open base with the bleed being spread over virtually the entire trailing edge thickness.

3. EXPERIMENTAL DETAILS

3.1 Model

The model (Fig. 1) was of hollow construction with the upper and lower portions separated by four slender streamlined spacers equally distributed across the span. A series of inlet choke plates which produced two dimensional slit intakes of various widths were used to regulate the mass flow through the model. The 1·6 mm diameter wire located just downstream from the choke plate (Fig. 1) was used to prevent the bleed flow from forming a wall jet attached to one side of the duct through the model. The bleed mass flow was measured with a six tube pitot rake and duct wall static tapping located near the model midspan. The effective base pressure was measured using a 1·6 mm diameter static probe supported from downstream. The static probe, which was located on the tunnel centreline, protruded into the model cavity with its pressure orifices in the plane of the base. To minimise the upstream influence of the static probe mounting, which unlike the probe itself would be subject to the full free stream flow velocity, a 10° included angle conical support starting 65 mm aft of the orifices was used.

The forward 31% of the model was of approximately semi-elliptic form and the remainder of the chord was parallel sided. The model thickness/chord ratio was 12·5% and the bleed aperture height/base height ratio was 93%. The model completely spanned the width of the tunnel and was supported by integral end tongues which passed through slots in optical glass windows in the tunnel sidewalls. Boundary layer trips consisting of spanwise bands of 0·15 mm carborundum particles attached with a thin (0·03 mm) layer of lacquer were used on both surfaces of the model. The bands were located 10 mm aft of the leading edge and were 2 mm wide, with a particle coverage of approximately 20%.

3.2 Wind Tunnel

The tests were carried out in the ARL transonic wind tunnel (Fig. 2) which has a test section 813 mm high and 533 mm wide. Solid sidewalls and longitudinally slotted top and bottom walls with an open area ratio of 16·5% at the model location were fitted. Mach number and dynamic pressure were derived from measurements of the pressure in the plenum chamber and in the contraction entry assuming these to be the static and total pressures of the test section flow respectively.

The model blockage ratio (model frontal area/test section area) was 1·9%. Due to the difficulty in predicting tunnel wall interference for models of this type no corrections were applied to the experimental data. The results of Reference 19 suggest that the blockage correction to Mach number should be less than $\Delta M = 0{\cdot}01$ at $M_0 = 0{\cdot}80$.

3.3 Test Program

The model was tested at zero incidence and Mach numbers of 0·50, 0·60, 0·70, 0·80, 0·85, 0·875, 0·90, 0·925, 0·95, 0·975, 1·00, 1·05, 1·10, 1·20, 1·30 and 1·35. The tunnel operating pressure was varied during the tests to achieve a reasonable compromise between holding the Reynolds number constant and utilizing the maximum Reynolds number available at each Mach number. The variation of test Reynolds number with Mach number is shown in Figure 3. At Mach numbers where the tunnel pressure was altered ($M_0 = 0{\cdot}50$, 0·70, 0·90 and 1·10) test points were taken at the higher and lower Reynolds number values.

Tests were carried out with the inlet sealed and with inlet slit widths (Fig. 1) of 0·38, 0·56,

0·64, 0·76, 0·94, 1·02, 1·14, 1·52, 1·91, 2·29 and 2·67 mm. These values were selected as the test program proceeded to give a reasonably even spread of bleed coefficients up to a maximum of 0·15.

Surface oil flow and schlieren observations indicated that the boundary layers approaching the trailing edge were turbulent under all test conditions. A pitot traverse of the boundary layer at the base was carried out at $M_0 = 0{\cdot}50$, $C_q = 0{\cdot}025$. The resulting velocity distribution showed a typical turbulent profile (Fig. 4) with a thickness of 2·10 mm and a momentum thickness of $\theta = 0{\cdot}217$ mm. Schlieren observations indicated that the boundary layer thickness was not significantly affected by Mach number or bleed mass flow.

3.4 Data Reduction

A preliminary calibration of the static probe used to measure base pressure showed it to be free from measurable error (error $< 0{\cdot}1\%$ of reading) under the conditions it would experience in the base flow. The static probe pressure was therefore used directly as the model base pressure P_b in the calculation of base pressure coefficient.

The bleed mass flow was calculated as follows: The local Mach number at each of the six pitot tubes (Fig. 1) was calculated using the static pressure from the duct wall tapping and the relevant pitot pressure. The local sonic velocity and density, and hence the local mass flux at each pitot location was calculated assuming the total temperature of the bleed flow to be equal to the free stream stagnation value. Using a least squares quadratic best fit to the six local mass flux values a total integrated mass flow was calculated.

4. RESULTS AND DISCUSSION

4.1 Base Pressure Measurements

A complete listing of the experimental results is presented in Table 1. In Figures 5 to 8 base pressure coefficient is plotted against bleed mass flow coefficient for the various test Mach numbers. At Mach numbers where the tunnel pressure was varied ($M_0 = 0{\cdot}50$, 0·70, 0·90 and 1·10) both high and low Reynolds number data are plotted. From Figures 5, 6 and 8 it can be seen that Reynolds number variations over the range covered by these tests had no significant effect on the results. The scatter evident in the plotted points is believed to be primarily due to small spanwise variations in the inlet slit causing some spanwise non uniformity in the bleed mass flow.

For Mach numbers up to 0·875 the curves of base pressure against bleed quantity show a pronounced knee where the base pressure rises rapidly for small increases in bleed (Figs 5 and 6). For Mach numbers in the range 0·90 to 1·00 the base pressure shows a smooth increase with increasing bleed (Figs 6 and 7). The sensitivity of the base pressure to small bleed quantities is considerably higher than that observed at lower speeds. For Mach numbers above 1·00 the base pressure shows an increase for low bleed quantities and a decrease for high bleed quantities (Figs 7 and 8). In some cases this high bleed-base pressure decrease was associated with the bleed air forming a wall jet and entering the base region in an unsymmetrical manner (Fig. 9). Some earlier supersonic bleed tests[11,12] suggest that the decrease in base pressure for large bleed quantities is a genuine effect of bleed. However due to the observed flow asymmetry in the present tests it is suggested that the large bleed supersonic results be treated with caution.

In Figure 10 the smoothed curves of Figures 5 to 8 are cross plotted to give curves of base pressure coefficient against Mach number for constant bleed mass flow coefficients. From this figure it can be seen that small bleed quantities produce particularly large drag reductions at Mach numbers near 0·90.

4.2 Schlieren Observations

A series of schlieren photographs of the base flow are reproduced in Figures 11 to 15. A vertical knife edge was used to show streamwise density gradients (dark for expansion, light for compression). When interpreting the schlieren photographs it should be noted that experience has shown that a lumpy appearance of the wake and the presence of wavelets moving upstream

over the model are strong indicators of vortex shedding. Due to the lack of spanwise correlation vortex streets are rarely clearly visible in high aspect ratio tests.

At a Mach number of 0·7 (Fig. 11) the $C_q = 0$ photograph shows clear evidence of the formation of a vortex street close to the base. For $C_q = 0{\cdot}05$ a small downstream displacement of the vortex formation point can be seen. As the bleed mass flow is increased through the knee of the C_{pb} *Vs* C_q curve (Centred at $C_q = 0{\cdot}06$ for $M_0 = 0{\cdot}7$) the vortex formation point is displaced rapidly downstream and the vortex strength appears to be reduced. The flow development illustrated in Figure 11 is typical of all test Mach numbers up to 0·90 where the surface shock waves reach the trailing edge. The downstream movement of the vortex formation point with increasing bleed quantity noted above has also been observed in low speed tests[9,10].

At a Mach number of 0·9 (Fig. 12) the model surface shock waves have moved downstream into the near wake where they appear to be interacting with the vortex formation region for $C_q = 0$. The apparent double shock waves evident in this figure are due to spanwise curvature of the shocks. For small bleed quantities ($C_q = 0{\cdot}018$ in Fig. 12) the shock waves are displaced slightly upstream and the vortex formation region slightly downstream so the two no longer interact. There is still clear evidence of strong vortex shedding. As the bleed mass flow is further increased ($C_q = 0{\cdot}048$ and 0·07 in Fig. 12) the shock waves move back onto the surface of the model and the vortex formation point moves downstream. The vortex strength also appears to be reduced.

At a Mach number of 0·925 (Fig. 13) a supersonic expansion at the trailing edge and normal shock waves interacting with the vortex formation region of the near wake are evident for $C_q = 0$. For $C_q = 0{\cdot}018$ the supersonic expansion is weakened and the normal shock waves and vortex formation region both displaced downstream. At higher bleed flows ($C_q = 0{\cdot}045$ and 0·066 in Fig. 13) a complex flow pattern develops. Weak oblique compression waves springing from the trailing edge effectively form the forward parts of λ feet on the main shock waves. The rear parts of the shocks reflect from the wake shear layers as expansions. Further downstream there is evidence of vortex formation and the wavelets formed in this region move upstream until they pile up against the supersonic region behind the reflected expansion.

The base flow for Mach numbers of 0·950 (Fig. 14) and 0·975 are similar to the $M_0 = 0{\cdot}925$ flow described above except that the expansion at the base becomes stronger and the terminal shock waves are more nearly normal to the wake at higher bleed mass flows. Strong vortex shedding is still evident at these Mach numbers for small bleed quantities.

At a Mach number near 1·00 the base flow changes its character significantly and remains basically unaltered for all higher test Mach numbers. This supersonic base flow is illustrated with the $M_0 = 1{\cdot}30$ photographs reproduced in Figure 15. For zero bleed there is a strong supersonic expansion at the trailing edge and the wake converges to a neck where the free shear layers merge without the formation of a strong vortex street. A pair of oblique shock waves spring from the neck of the wake. As the bleed flow is increased the base expansion is weakened, the angle of convergence of the wake is reduced and the shock waves are weakened. For a bleed mass flow of $C_q = 0{\cdot}05$ the shock waves appear to have vanished entirely. The supersonic base flow development described here is very similar to that observed in other supersonic tests[11,13].

4.3 Comparison with other Results

In Figure 16 the $M_0 = 0{\cdot}5$ curve of base pressure coefficient against bleed mass flow coefficient from the current tests is compared with the low speed results of References 9 and 10. From this figure it can be seen that the general form of the three results is similar although the numerical values differ significantly. These differences can be explained by considering the details of the experimental arrangements used. The model used in Reference 10 employed a porous base which behaved essentially as a solid base for $C_q = 0$ whereas the model used here had an open base. Previous work[18] has shown that base geometries employing open cavities have less drag than solid bases. As would be expected from the above considerations the present results show a higher value of base pressure than the results of Reference 10 for all bleed quantities. The tests reported in Reference 9 were carried out on a model with an aspect ratio of 0·7. At this low aspect ratio the tunnel sidewall boundary layers would be expected to produce a significant three dimensional bleed flow into the base region. This effect would be particularly significant for small values of C_q when the base pressure was low. The comparison in Figure 16

clearly shows the effect of the low aspect ratio on the results of Reference 9. For low values of C_q the base pressure coefficient from Reference 9 is well below that of Reference 10 and the present tests. At high bleed rates this difference in base pressure coefficient is reduced.

In Figure 17 the $M_0 = 1{\cdot}10$, $1{\cdot}20$ and $1{\cdot}35$ results from the current tests are compared with the results of References 13 and 14 (at $M_0 = 2{\cdot}025$ and $2{\cdot}21$ respectively). The tests reported in References 11 and 12 employed bleed injection through narrow slots and the results are not reproduced here since the base geometries were considered to be sufficiently different to render comparisons valueless. The bleed flow coefficient used originally in Reference 13 was defined as: "$C_q = Q/p_i a_i S$ où Q représente le débit masse du flux secondaire, S la surface du culot, p_i et a_i la masse spécifique et la vitesse du son relatives aux conditions génératrices de l'écoulement extérieur". In calculating the equivalent bleed flow coefficient as defined in the present note p_i and a_i were taken as stagnation values isentropically related to the free stream conditions. In References 6 and 14 p_i and a_i appear to have been interpreted as free stream values. The base pressure data in Reference 14 were presented in the form of percentage changes in the zero bleed base pressure. To convert the data into a form suitable for comparison a zero bleed base pressure was derived from References 12 and 13. From Figure 17 it can be seen that the present low supersonic results appear to be consistent with other supersonic data.

In Figure 18 the present base bleed results are compared with the best serrated base configuration from Reference 7. From this Figure it can be seen that the use of a bleed mass flow coefficient of approximately $0{\cdot}07$ produces a higher base pressure coefficient (lower base drag) than the best serrated base configuration over the entire test Mach number range. The practicality of providing a bleed flow of this magnitude on an aircraft would have to be determined for each particular design.

On the basis of the work presented in Reference 7 it appears highly probable that the total bleed quantity required to achieve a given drag reduction could be greatly reduced by using discrete spanwise cells of bleed with solid downstream protrusions between them.

5. CONCLUSION

Measurements of the effect of base bleed on base pressure coefficient have been carried out on a two dimensional model in the ARL transonic wind tunnel. The test Mach number range was $0{\cdot}5 \leqslant M_0 \leqslant 1{\cdot}35$, the Reynolds number (based on trailing edge thickness) was approximately 9×10^4 and the surface boundary layers were turbulent with a ratio of (base height/separation point boundary layer momentum thickness) equal to 70. In addition to pressure measurements a series of schlieren photographs were taken to illustrate the base flow development through the transonic speed range.

A novel experimental arrangement with the bleed flow derived from an inlet slit in the model leading edge was used. The subsonic and supersonic data obtained were consistent with other published results. The transonic data, which appears to be unique, can therefore be viewed with some confidence.

The results indicate that a bleed mass flow coefficient of about $0{\cdot}07$ produces a lower base drag than the best practical non bleed base geometry. The application of base bleed to blunt trailing edge wings involves considerations of wing structural design to accommodate the bleed ducts and the effective drag penalty of the bleed momentum.

It appears probable that the required bleed quantities could be reduced by the use of discrete spanwise cells of bleed with suitable base contouring between the bleed cells.

REFERENCES

1. Pearcey, H. H. — The Aerodynamic Design of Section Shapes for Swept Wings. Advances in Aeronautical Sciences, Vol. 3. Proc. 2nd Int. Congr. Aer. Sci. Zurich, 1960. Pergamon Press 1962.
2. Holder, D. W. — The Transonic Flow Past Two Dimensional Aerofoils. J. Royal Aero. Soc., Vol. 68. August 1964.
3. Pollock, N. — Two Dimensional Aerofoils at Transonic Speeds. ARL Aero. Note 314, 1968.
4. Whitcomb, R. T. — Review of NASA Supercritical Aerofoils. ICAS Paper 74–10, 1974.
5. Fulker, J. L. — Aerodynamic Data for RAE 9550, A Supercritical Aerofoil. RAE TR 75068, 1975.
6. Tanner, M. — Reduction of Base Drag. Prog. Aerospace Sci., Vol. 16. D. Küchemann, Ed. Pergamon Press, 1975.
7. Pollock, N. — Segmented Blunt Trailing Edges at Subsonic and Transonic Speeds. ARL Aero. Rpt. 137, 1972.
8. Tanner, M. — A method for Reducing the Base Drag of Wings with Blunt Trailing Edge. Aero. Quart., Vol. 23, Part 1, 1972.
9. Wood, C. J. — The Effect of Base Bleed on a Periodic Wake. J. Royal Aero. Soc., Vol. 68, July 1964.
10. Bearman, P. W. — The Effect of Base Bleed on the Flow Behind a Two-Dimensional Model with a Blunt Trailing Edge. Aero. Quart., Vol. 18, August 1967.
11. Wimbrow, W. R. — Effects of Base Bleed on the Base Pressure of Blunt-Trailing-Edge Airfoils at Supersonic Speeds. NACA, RM, A54A07, March 1954.
12. Fuller, L. and Reid, J. — Experiments on Two-Dimensional Base Flow at $M = 2{\cdot}4$. ARC, R & M 3064, 1958.
13. Sirex, M. — Pression de Culot et Processus de Mélange Turbulent en Écoulement Supersonique Plan. La Recherche Aéronautique, No. 78, Sept.-Oct. 1960.
14. Ginoux, J. J. — Effect of Gas Injection in Separated Supersonic Flows. TCEA, Tech. Note 7, Feb. 1962.
15. Bearman, P. W. — Investigation of the Flow Behind a Two-Dimensional Model with a Blunt Trailing Edge and Fitted with Splitter Plates. J. Fluid Mech. Vol. 21, Part 2, 1965.
16. Ginoux, J. J. — On the Existence of Cross-Flows in Separated Supersonic Streams. TCEA Tech. Note 6, Feb. 1962.
17. Pollock, N. — Some Effects of Base Geometry on Two-Dimensional Base Drag at Subsonic and Transonic Speeds. ARL Areo. Note 316, Oct. 1969.
18. Nash, J. F., Quincey, V. G. and Callinan, J. — Experiments on Two-Dimensional Base Flow at Subsonic and Transonic Speeds. ARC, R & M 3427, 1966.
19. Fairlie, B. D., and Pollock, N. — Evaluation of Wall Interference Effects in a Two-Dimensional Transonic Wind Tunnel by Subsonic Linear Theory. ARL, Aero. Rpt. To be published.

TABLE 1
Experimental Results

M_0	R_e	C_q	C_{pb}
0·50	10·0 × 10^4	0	−0·473
,,	,,	0·024	−0·408
,,	,,	0·035	−0·409
,,	,,	0·036	−0·396
,,	,,	0·062	−0·338
,,	,,	0·064	−0·348
,,	,,	0·069	−0·283
,,	,,	0·073	−0·228
,,	,,	0·097	−0·144
,,	,,	0·136	−0·111
,,	,,	0·146	−0·121
0·50	8·0 × 10^4	0	−0·468
,,	,,	0·025	−0·410
,,	,,	0·029	−0·413
,,	,,	0·035	−0·395
,,	,,	0·037	−0·395
,,	,,	0·061	−0·338
,,	,,	0·062	−0·356
,,	,,	0·068	−0·289
,,	,,	0·076	−0·228
,,	,,	0·098	−0·140
,,	,,	0·135	−0·110
,,	,,	0·147	−0·118
0·60	9·0 × 10^4	0	−0·480
,,	,,	0·020	−0·429
,,	,,	0·028	−0·434
,,	,,	0·034	−0·424
,,	,,	0·061	−0·372
,,	,,	0·062	−0·352
,,	,,	0·063	−0·272
,,	,,	0·070	−0·220
,,	,,	0·093	−0·148
,,	,,	0·130	−0·125
,,	,,	0·135	−0·130
0·70	9·8 × 10^4	0	−0·521
,,	,,	0·026	−0·466
,,	,,	0·033	−0·467
,,	,,	0·041	−0·450
,,	,,	0·058	−0·380
,,	,,	0·059	−0·337
,,	,,	0·063	−0·268
,,	,,	0·068	−0·215
,,	,,	0·089	−0·170
,,	,,	0·117	−0·153
,,	,,	0·126	−0·140
0·70	8·9 × 10^4	0	−0·524
,,	,,	0·026	−0·469
,,	,,	0·034	−0·453
,,	,,	0·036	−0·470
,,	,,	0·057	−0·385

TABLE 1 (*Continued*)

M_0	R_e	C_q	C_{pb}
0·70	8·9 × 10⁴	0·059	−0·344
,,	,,	0·063	−0·269
,,	,,	0·067	−0·216
,,	,,	0·089	−0·173
,,	,,	0·120	−0·151
,,	,,	0·127	−0·138
0·80	9·5 × 10⁴	0	−0·557
,,	,,	0·018	−0·489
,,	,,	0·029	−0·505
,,	,,	0·034	−0·463
,,	,,	0·053	−0·370
,,	,,	0·054	−0·316
,,	,,	0·059	−0·264
,,	,,	0·064	−0·225
,,	,,	0·085	−0·179
,,	,,	0·115	−0·151
,,	,,	0·119	−0·150
0·85	9·7 × 10⁴	0	−0·579
,,	,,	0·023	−0·497
,,	,,	0·028	−0·518
,,	,,	0·030	−0·467
,,	,,	0·053	−0·345
,,	,,	0·056	−0·305
,,	,,	0·056	−0·260
,,	,,	0·066	−0·230
,,	,,	0·085	−0·182
,,	,,	0·116	−0·150
,,	,,	0·120	−0·144
0·875	9·8 × 10⁴	0	−0·563
,,	,,	0·023	−0·476
,,	,,	0·024	−0·513
,,	,,	0·034	−0·450
,,	,,	0·051	−0·310
,,	,,	0·054	−0·242
,,	,,	0·055	−0·267
,,	,,	0·064	−0·215
,,	,,	0·084	−0·177
,,	,,	0·114	−0·137
,,	,,	0·116	−0·147
0·90	9·9 × 10⁴	0	−0·530
,,	,,	0·020	−0·408
,,	,,	0·029	−0·444
,,	,,	0·029	−0·341
,,	,,	0·051	−0·240
,,	,,	0·054	−0·227
,,	,,	0·055	−0·209
,,	,,	0·062	−0·174
,,	,,	0·084	−0·144
,,	,,	0·109	−0·111
,,	,,	0·113	−0·127
0·90	8·5 × 10⁴	0	−0·509

TABLE 1 (*Continued*)

M_0	R_e	C_q	C_{pb}
0·90	$8{\cdot}5 \times 10^4$	0·019	−0·403
,,	,,	0·025	−0·458
,,	,,	0·026	−0·342
,,	,,	0·052	−0·243
,,	,,	0·054	−0·224
,,	,,	0·058	−0·198
,,	,,	0·065	−0·173
,,	,,	0·082	−0·144
,,	,,	0·108	−0·119
,,	,,	0·114	−0·118
0·925	$8{\cdot}6 \times 10^4$	0	−0·608
,,	,,	0·016	−0·486
,,	,,	0·024	−0·524
,,	,,	0·027	−0·451
,,	,,	0·054	−0·332
,,	,,	0·056	−0·323
,,	,,	0·060	−0·272
,,	,,	0·062	−0·238
,,	,,	0·084	−0·217
,,	,,	0·092	−0·158
,,	,,	0·115	−0·157
0·95	$8{\cdot}7 \times 10^4$	0	−0·722
,,	,,	0·019	−0·608
,,	,,	0·023	−0·482
,,	,,	0·028	−0·568
,,	,,	0·045	−0·381
,,	,,	0·054	−0·365
,,	,,	0·055	−0·341
,,	,,	0·061	−0·307
,,	,,	0·062	−0·255
,,	,,	0·082	−0·272
,,	,,	0·082	−0·242
0·975	$8{\cdot}8 \times 10^4$	0	−0·834
,,	,,	0·016	−0·590
,,	,,	0·022	−0·649
,,	,,	0·022	−0·557
,,	,,	0·044	−0·503
,,	,,	0·054	−0·480
,,	,,	0·054	−0·431
,,	,,	0·060	−0·398
,,	,,	0·067	−0·312
,,	,,	0·070	−0·400
,,	,,	0·086	−0·354
1·00	$8{\cdot}9 \times 10^4$	0	−0·831
,,	,,	0·021	−0·633
,,	,,	0·024	−0·678
,,	,,	0·032	−0·607
,,	,,	0·047	−0·567
,,	,,	0·052	−0·541
,,	,,	0·055	−0·532
,,	,,	0·064	−0·499

TABLE 1 (*Continued*)

M_0	R_e	C_q	C_{pb}
1·00	8·9 × 10⁴	0·076	−0·506
,,	,,	0·079	−0·477
,,	,,	0·083	−0·436
1·05	9·0 × 10⁴	0	−0·739
,,	,,	0·023	−0·604
,,	,,	0·025	−0·565
,,	,,	0·031	−0·538
,,	,,	0·049	−0·511
,,	,,	0·051	−0·453
,,	,,	0·051	−0·508
,,	,,	0·058	−0·489
,,	,,	0·063	−0·480
,,	,,	0·076	−0·579
,,	,,	0·079	−0·542
1·10	9·2 × 10⁴	0	−0·659
,,	,,	0·025	−0·530
,,	,,	0·025	−0·496
,,	,,	0·032	−0·474
,,	,,	0·049	−0·442
,,	,,	0·051	−0·433
,,	,,	0·055	−0·389
,,	,,	0·058	−0·414
,,	,,	0·063	−0·406
,,	,,	0·076	−0·506
,,	,,	0·080	−0·479
1·10	5·8 × 10⁴	0	−0·661
,,	,,	0·015	−0·542
,,	,,	0·024	−0·502
,,	,,	0·032	−0·483
,,	,,	0·052	−0·437
,,	,,	0·054	−0·438
,,	,,	0·059	−0·425
,,	,,	0·062	−0·384
,,	,,	0·065	−0·415
,,	,,	0·078	−0·494
,,	,,	0·080	−0·401
1·20	6·0 × 10⁴	0	−0·496
,,	,,	0·022	−0·347
,,	,,	0·023	−0·379
,,	,,	0·028	−0·320
,,	,,	0·051	−0·280
,,	,,	0·054	−0·255
,,	,,	0·055	−0·273
,,	,,	0·059	−0·215
,,	,,	0·066	−0·256
,,	,,	0·078	−0·331
,,	,,	0·081	−0·292
1·30	6·1 × 10⁴	0	−0·432
,,	,,	0·022	−0·330
,,	,,	0·025	−0·300
,,	,,	0·033	−0·278

TABLE 1 (*Continued*)

M_0	R_e	C_q	C_{pb}
1·30	6·1 × 10^4	0·053	−0·247
,,	,,	0·054	−0·238
,,	,,	0·061	−0·226
,,	,,	0·066	−0·210
,,	,,	0·067	−0·219
,,	,,	0·079	−0·315
,,	,,	0·082	−0·286
1·35	6·2 × 10^4	0	−0·402
,,	,,	0·026	−0·280
,,	,,	0·028	−0·304
,,	,,	0·037	−0·255
,,	,,	0·054	−0·227
,,	,,	0·056	−0·219
,,	,,	0·061	−0·212
,,	,,	0·065	−0·209
,,	,,	0·067	−0·204
,,	,,	0·080	−0·301
,,	,,	0·083	−0·279

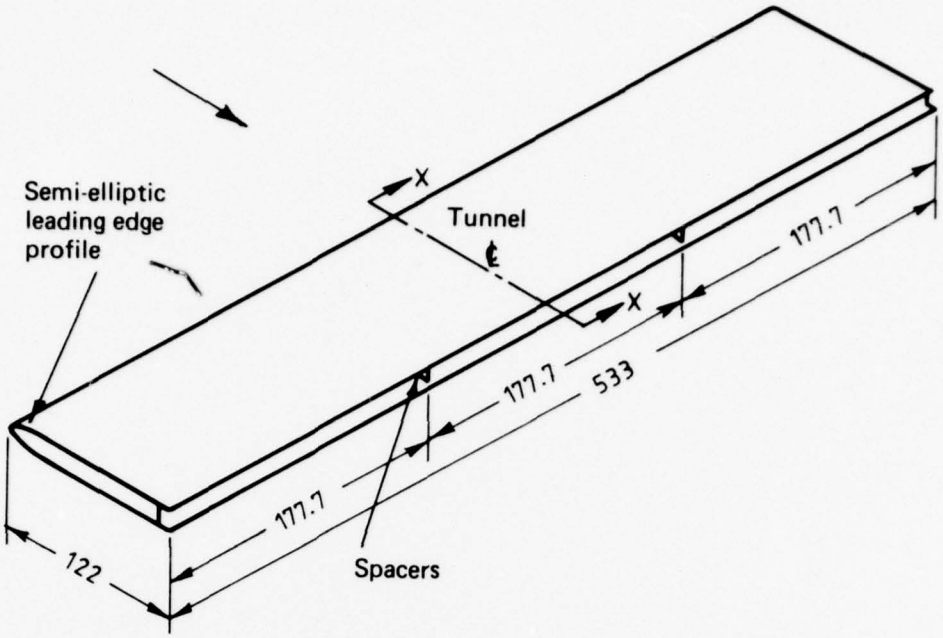

Section X--X

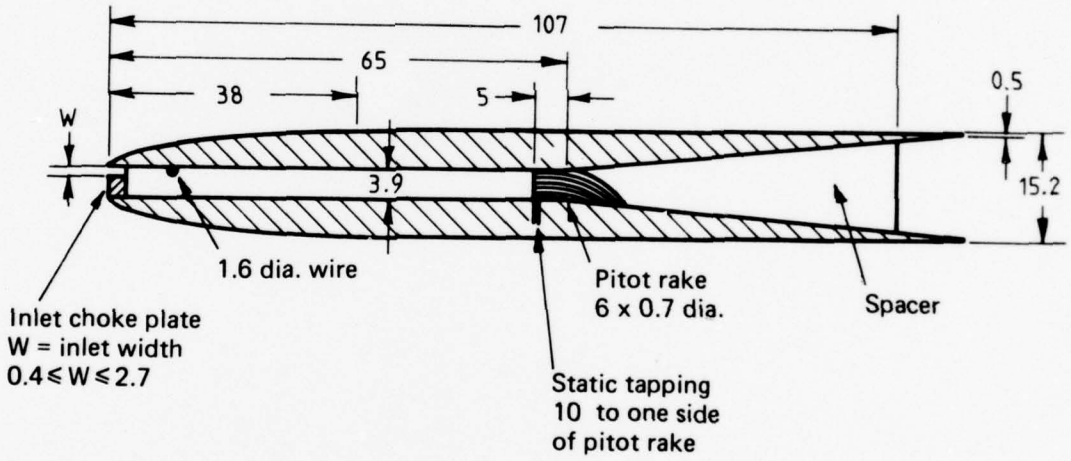

Note: all dimensions in m m

FIG. 1. DETAILS OF MODEL

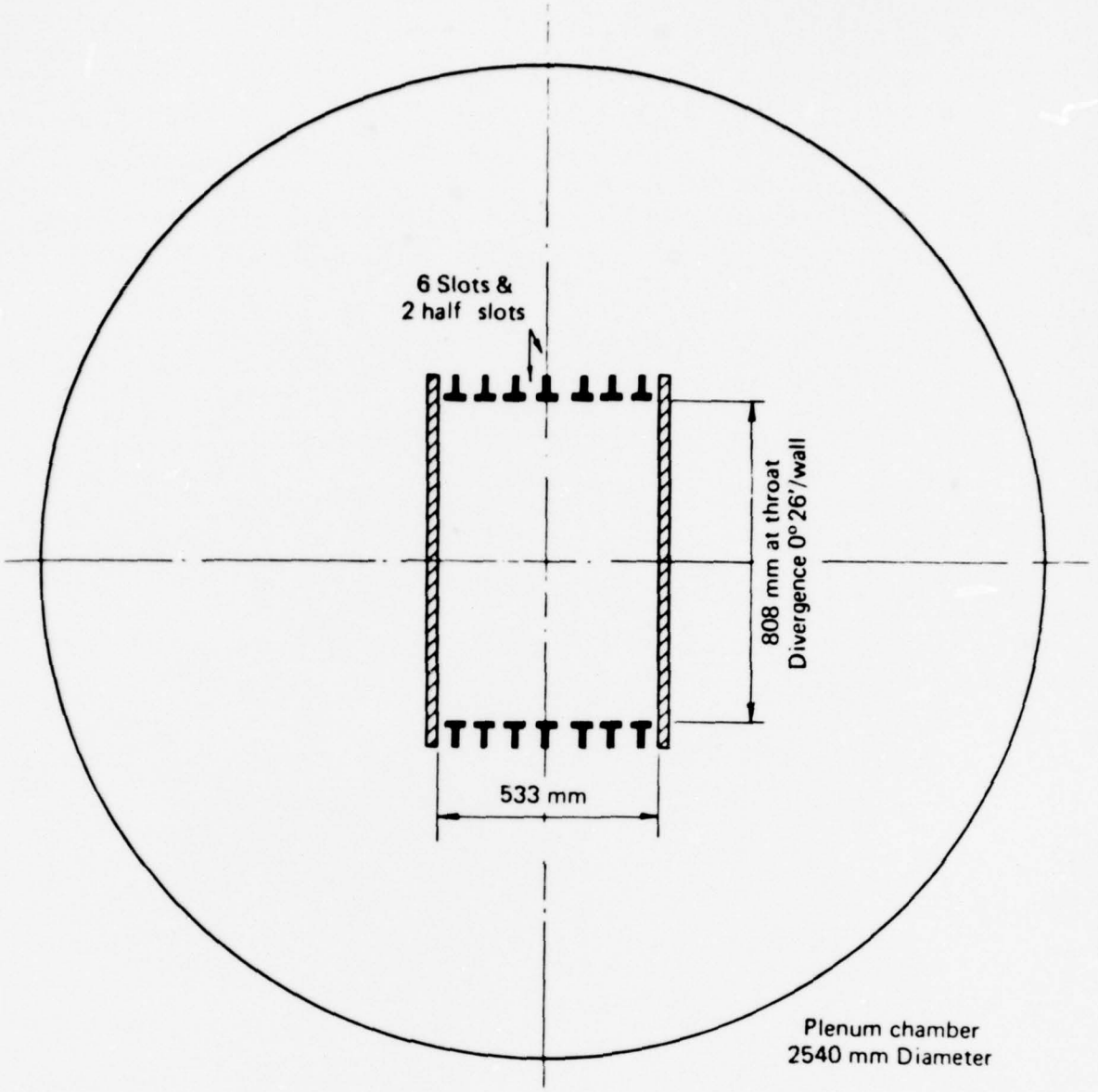

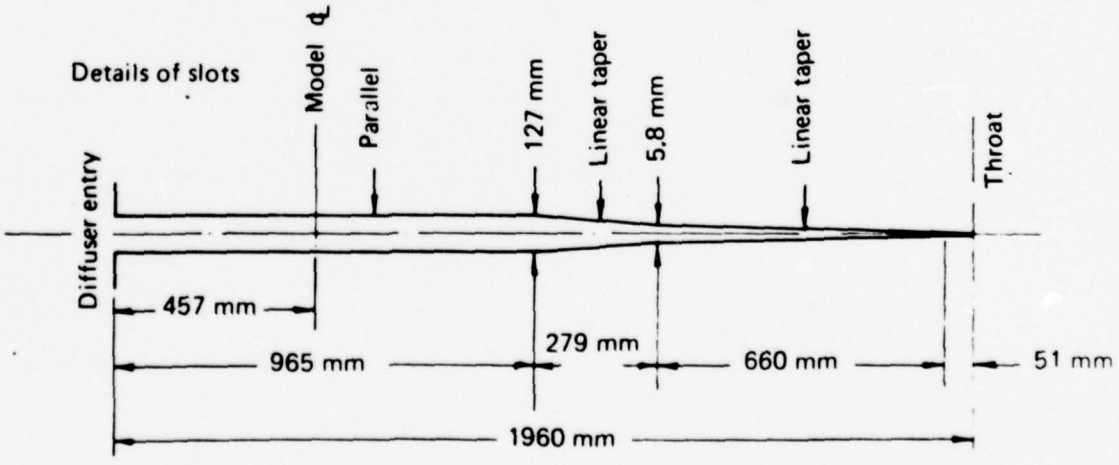

FIG. 2 DETAILS OF SLOTTED WORKING SECTION

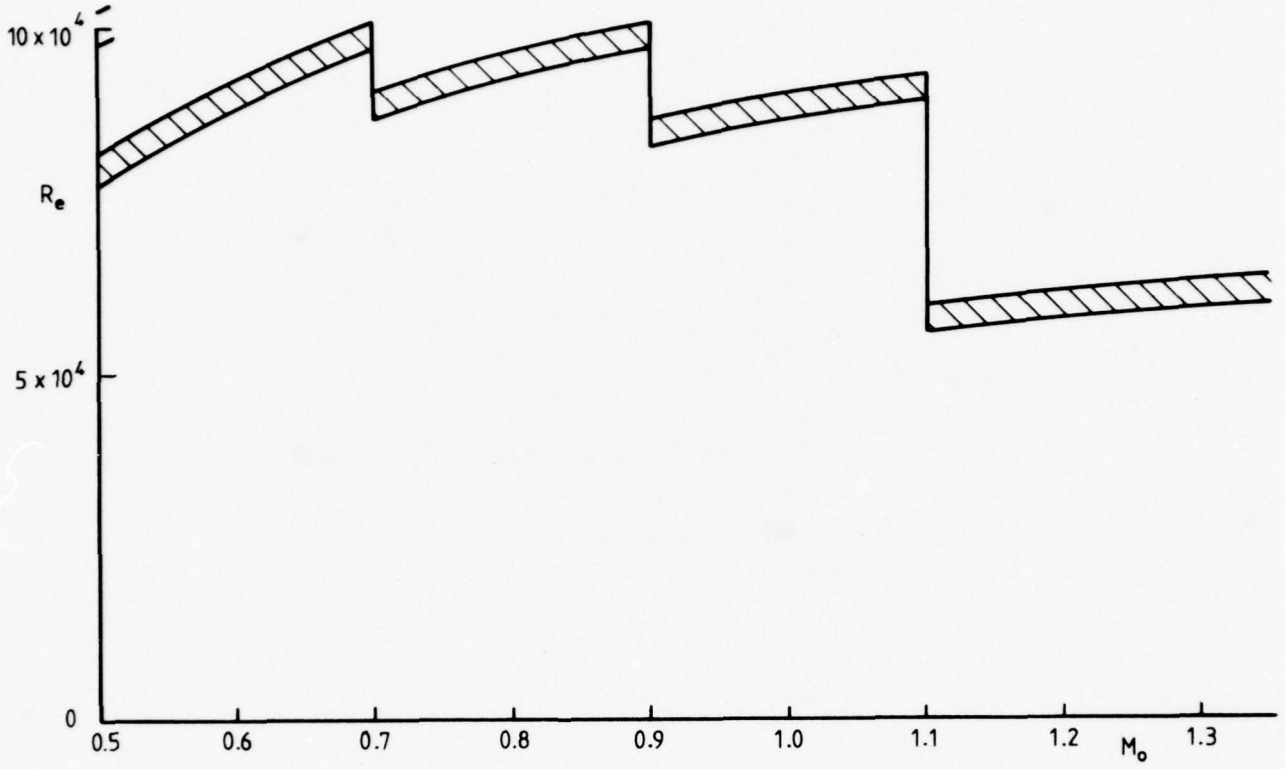

FIG. 3. VARIATION OF TEST REYNOLDS NUMBER WITH MACH NUMBER

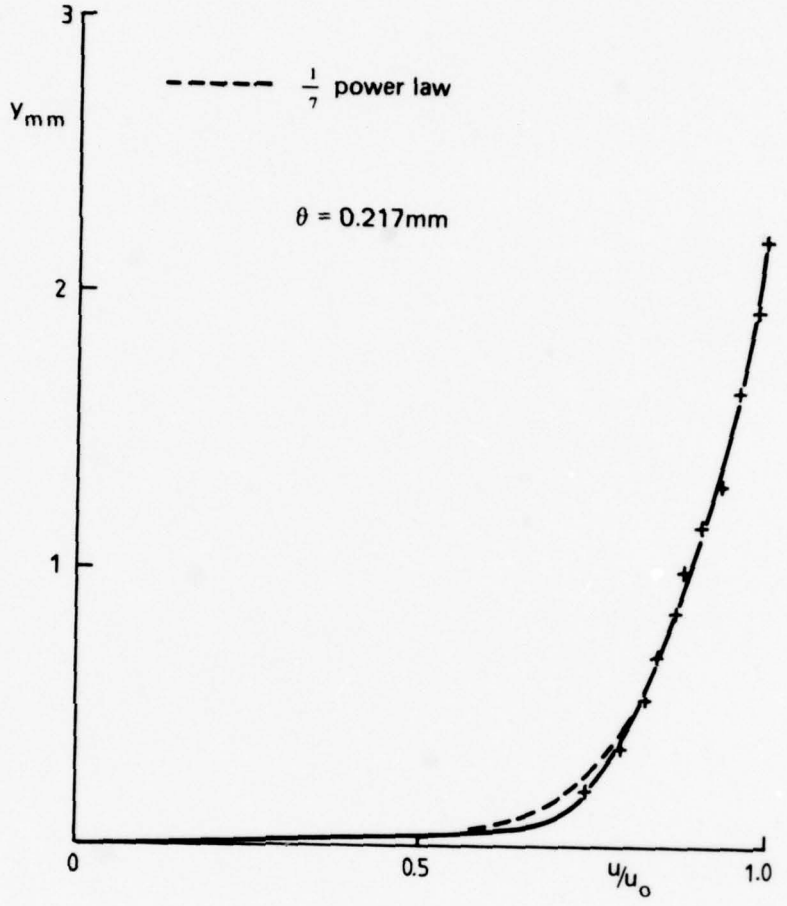

FIG. 4. BOUNDARY LAYER PROFILE AT BASE (M_o = 0.50, Cq = 0.025)

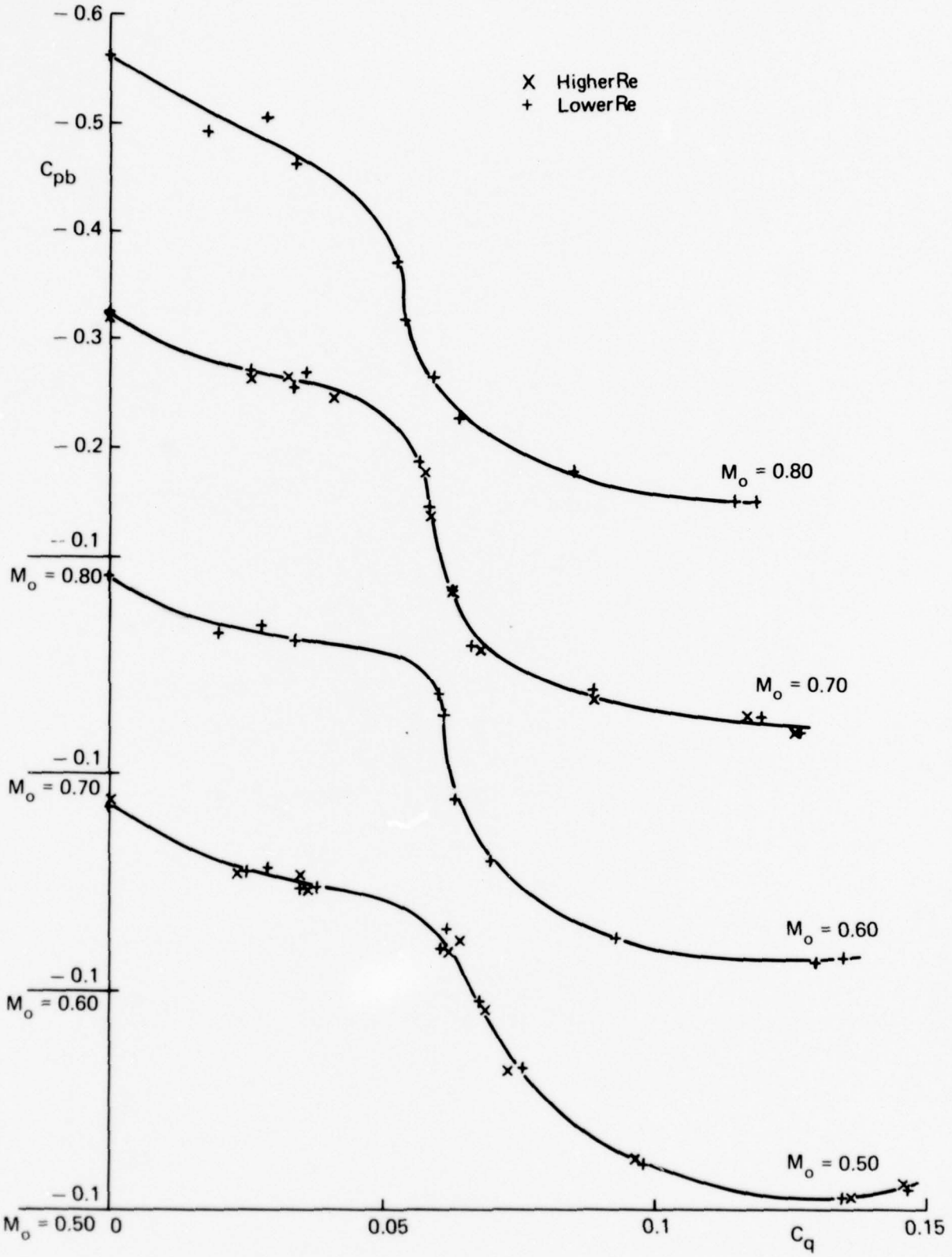

FIG. 5. VARIATION OF BASE PRESSURE WITH BLEED MASS FLOW

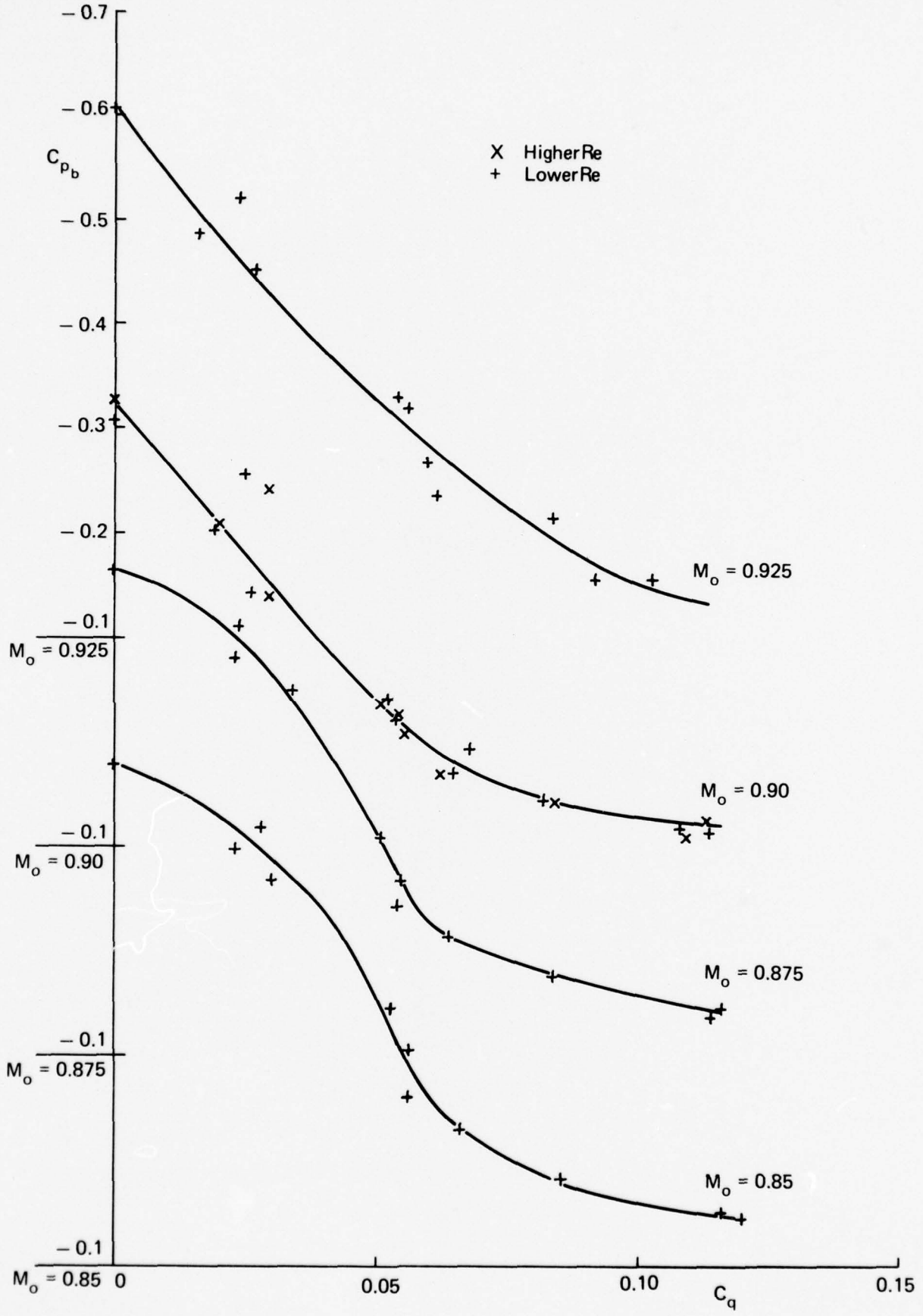

FIG. 6. VARIATION OF BASE PRESSURE WITH BLEED MASS FLOW

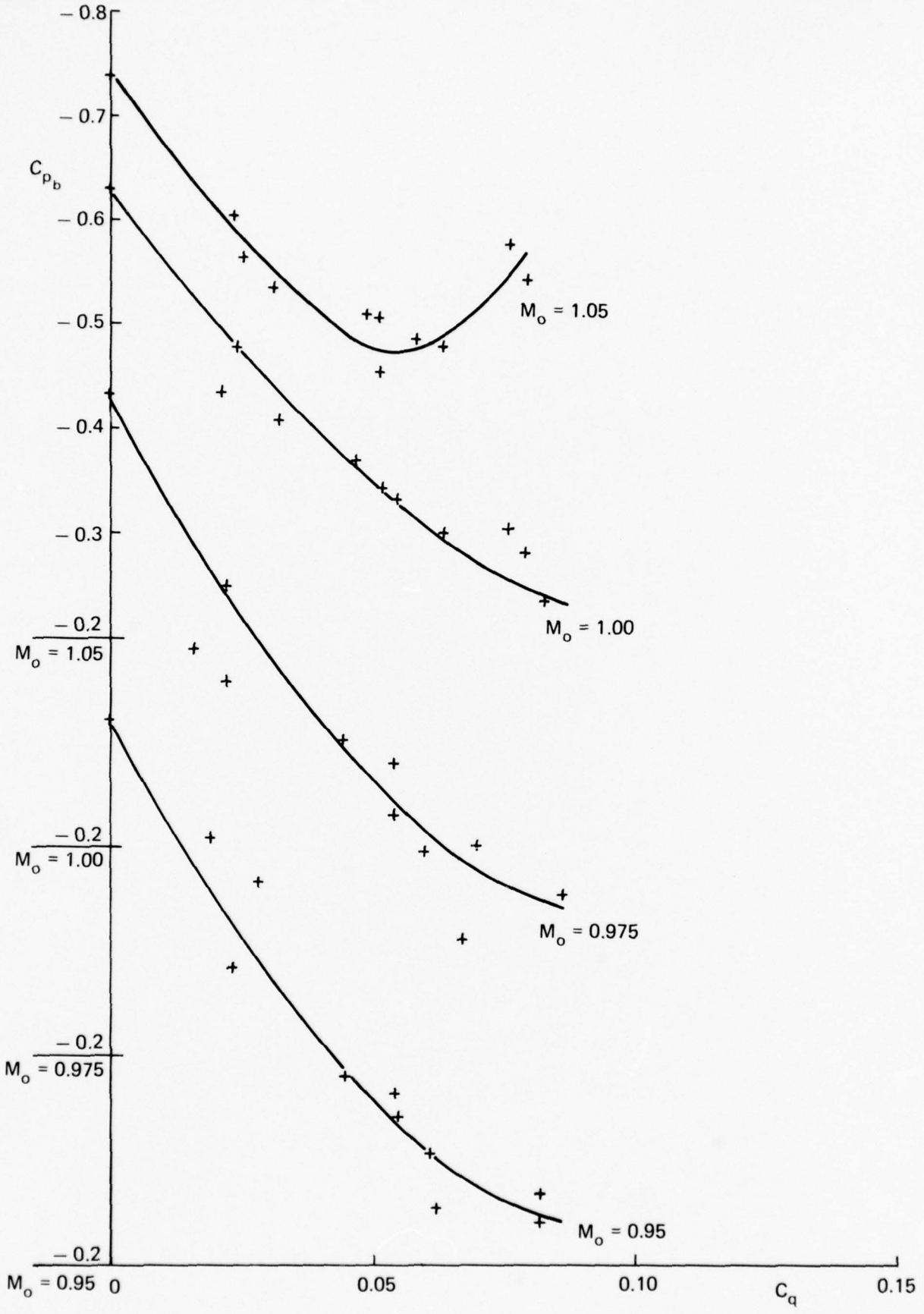

FIG. 7. VARIATION OF BASE PRESSURE WITH BLEED MASS FLOW

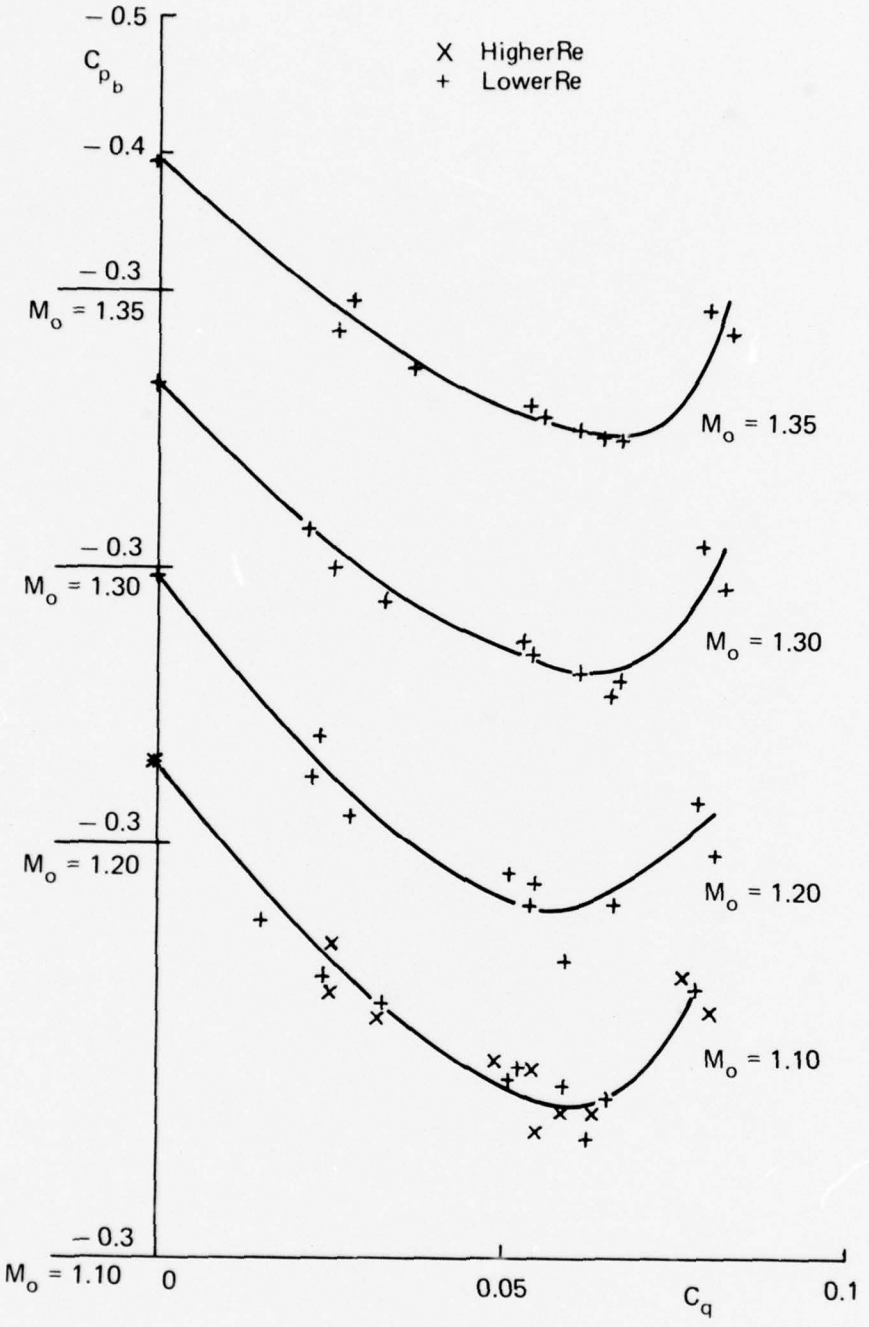

FIG. 8. VARIATION OF BASE PRESSURE WITH BLEED MASS FLOW

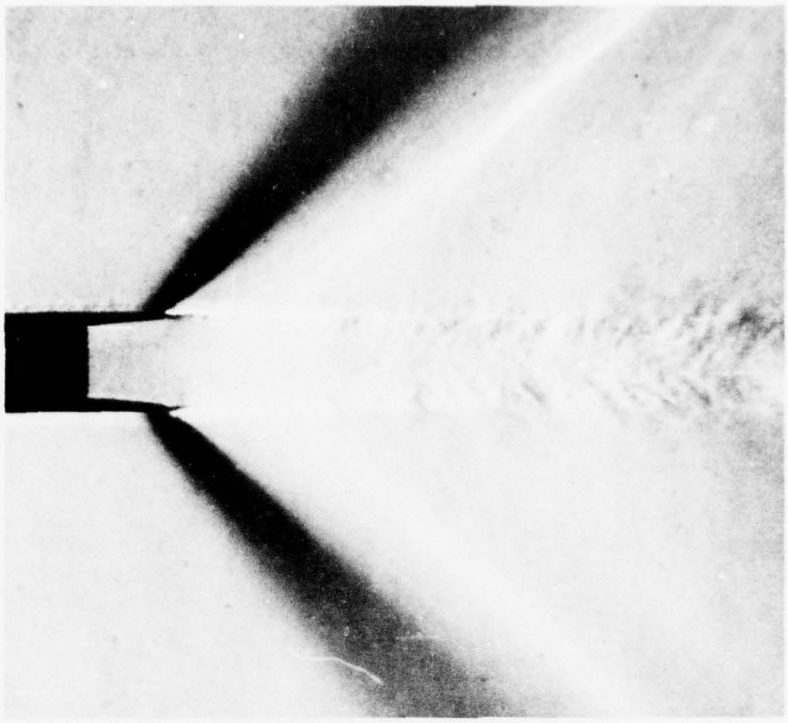

$C_q = 0.055 \quad C_{\bar{p}_b} - 0.25$

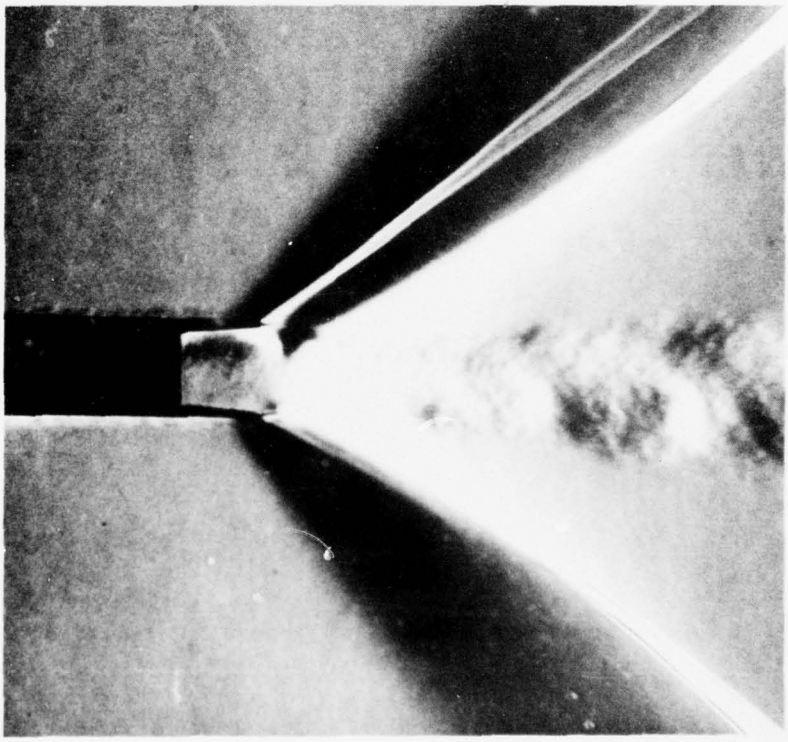

$C_q = 0.09 \quad C_{\bar{p}_b} - 0.45$

FIG. 9. SCHLIEREN PHOTOGRAPHS OF BASE FLOW $M_o = 1.20$

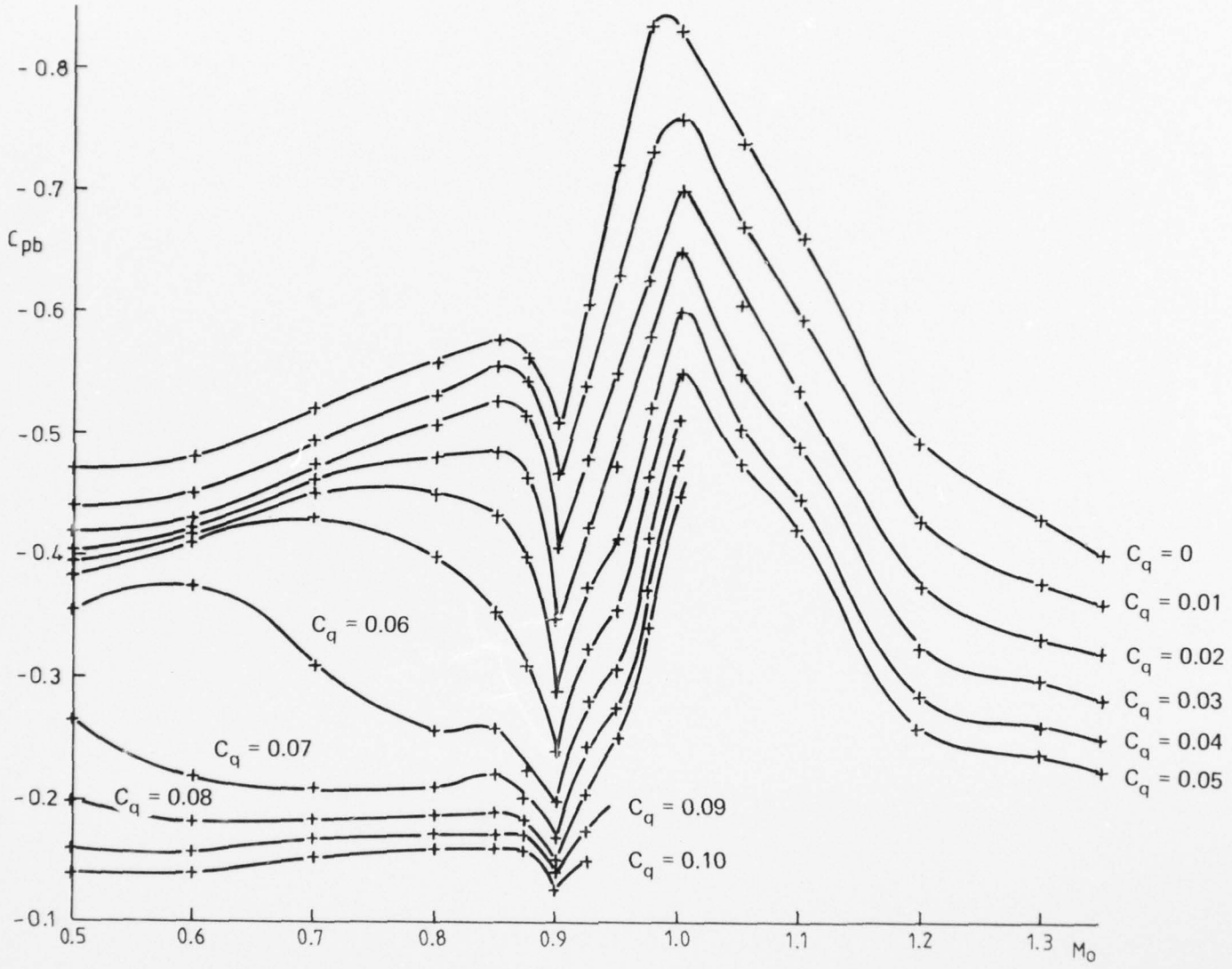

FIG. 10. VARIATION OF BASE PRESSURE WITH MACH NUMBER

$C_q = 0$ $C_{p_b} = -0.552$

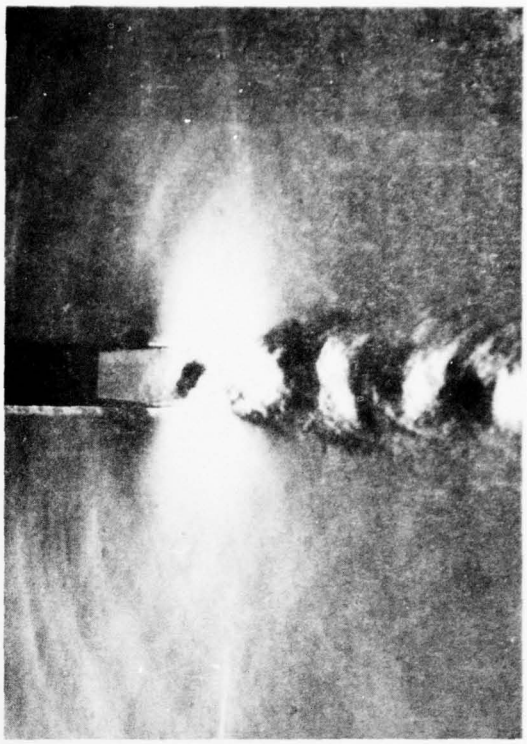

$C_q = 0.05$ $C_{p_b} = -0.430$

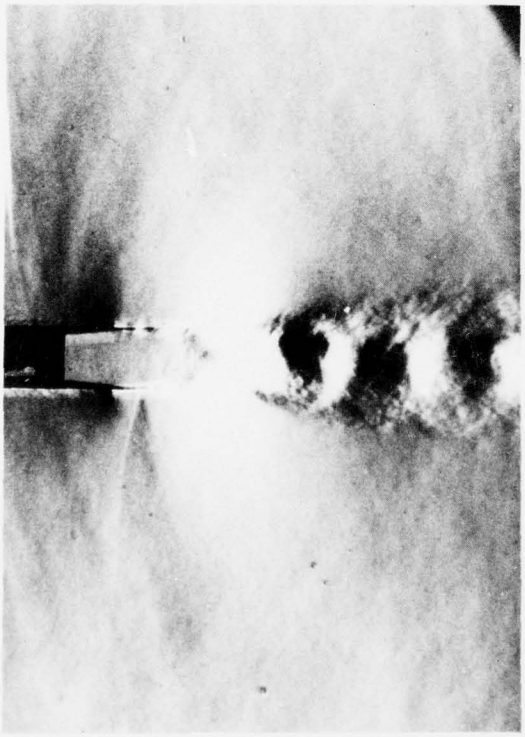

$C_q = 0.062$ $C_{p_b} = -0.281$

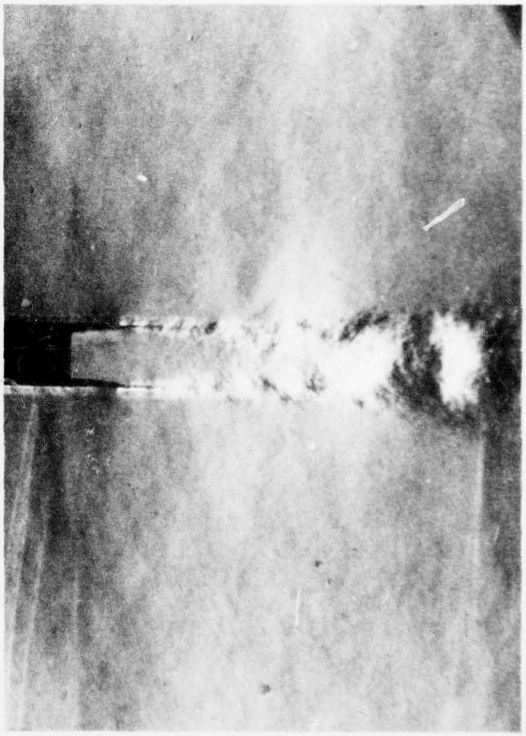

$C_q = 0.068$ $C_{p_b} = -0.220$

FIG. 11. SCHLIEREN PHOTOGRAPHS OF BASE FLOW $M_o = 0.70$

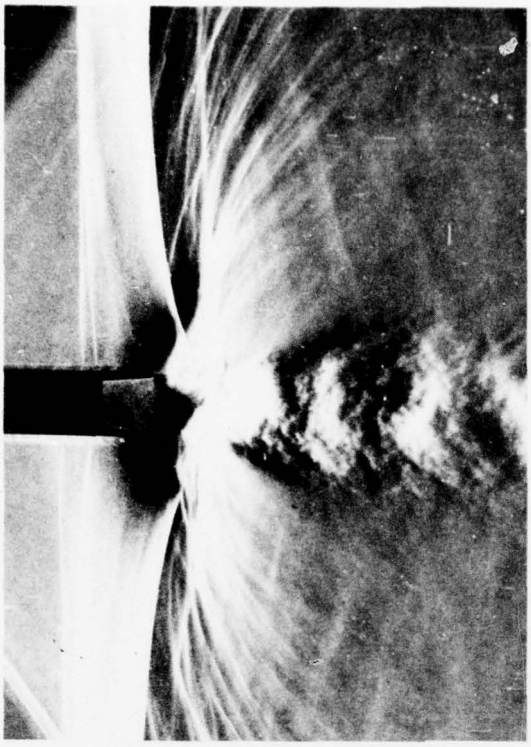

$C_q = 0 \quad C_{p_b} = -0.523$

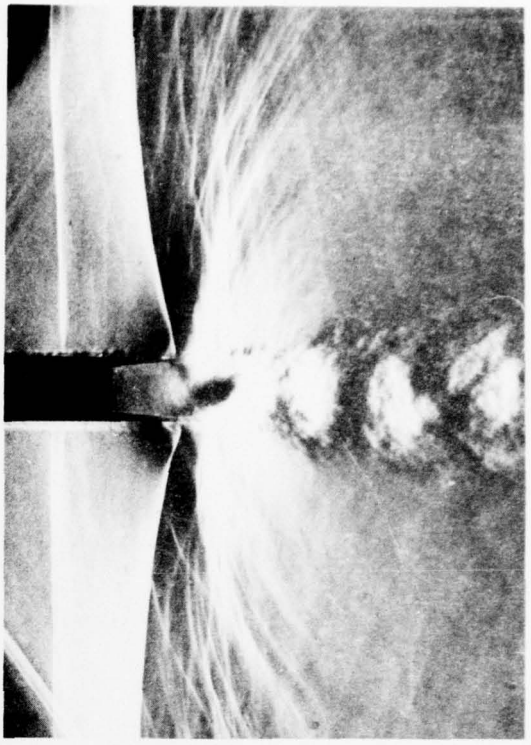

$C_q = 0.018 \quad C_{p_b} = -0.416$

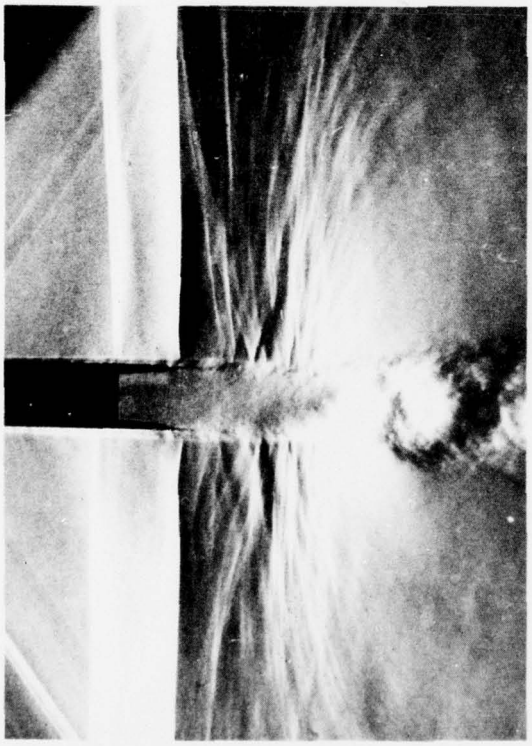

$C_q = 0.048 \quad C_{p_b} = -0.250$

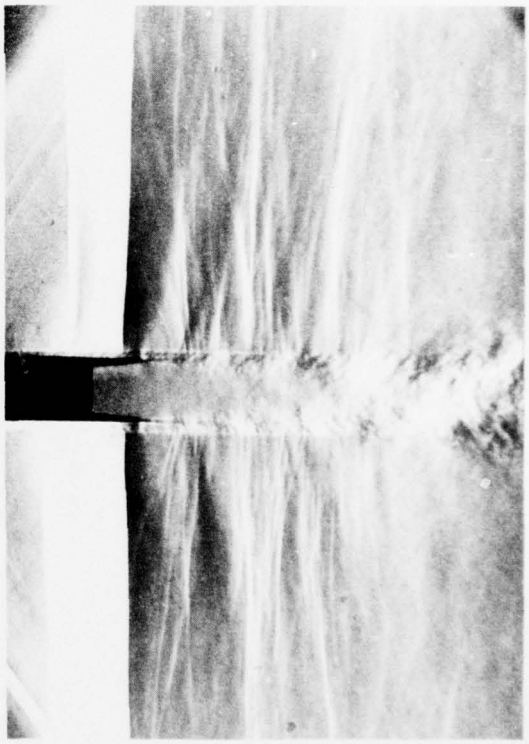

$C_q = 0.07 \quad C_{p_b} = -0.170$

FIG. 12. SCHLIEREN PHOTOGRAPHS OF BASE FLOW $M_o = 0.90$

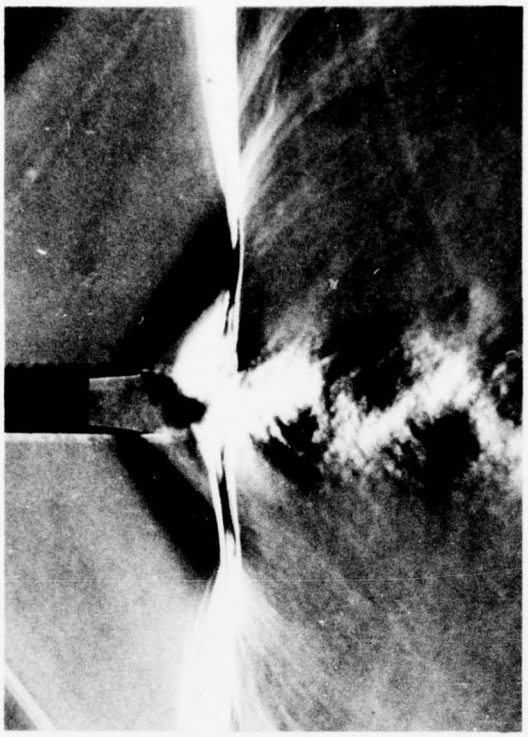

$C_q = 0 \quad C_{p_b} = -0.599$

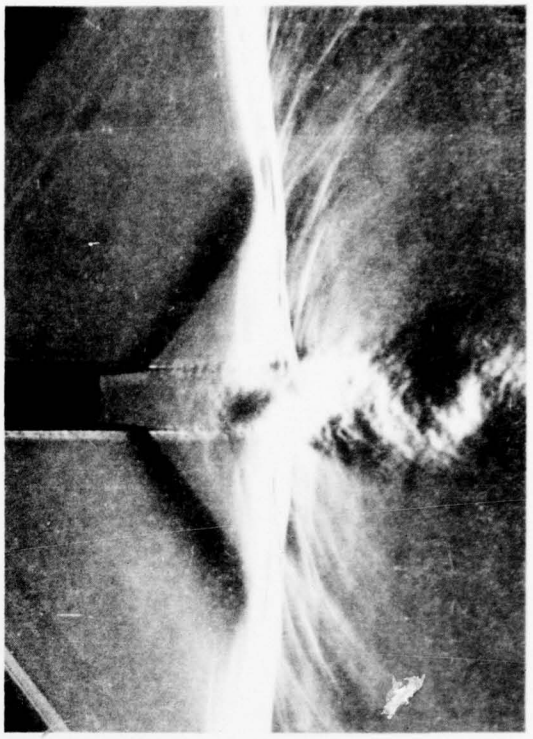

$C_q = 0.018 \quad C_{p_b} = -0.488$

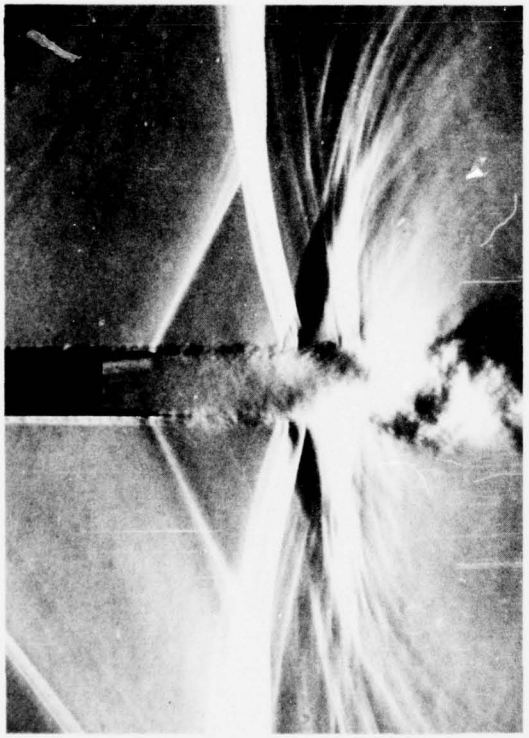

$C_q = 0.045 \quad C_{p_b} = -0.349$

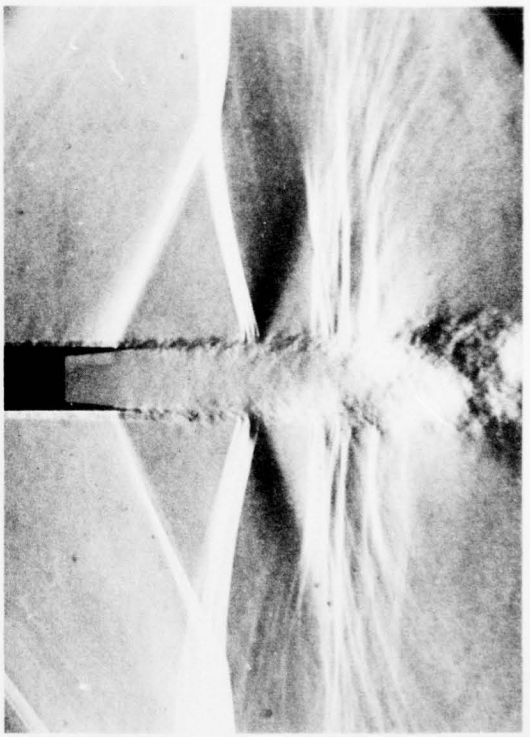

$C_q = 0.066 \quad C_{p_b} = -0.258$

FIG. 13. SCHLIEREN PHOTOGRAPHS OF BASE FLOW $M_o = 0.925$

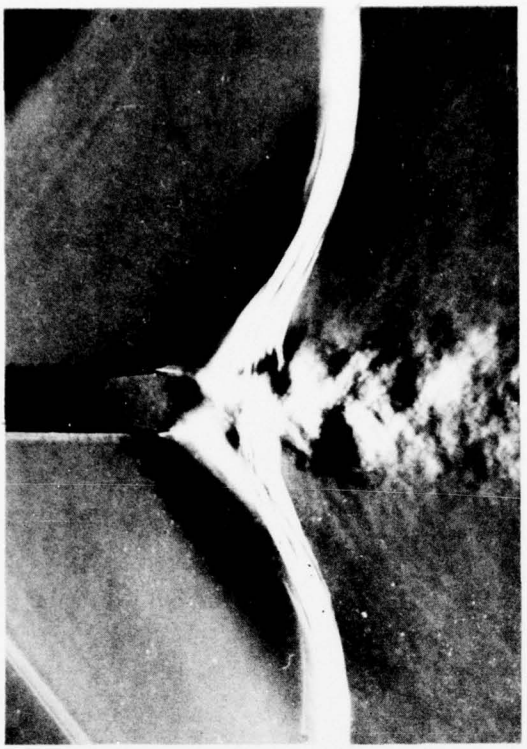

$C_q = 0 \quad C_{p_b} = -0.728$

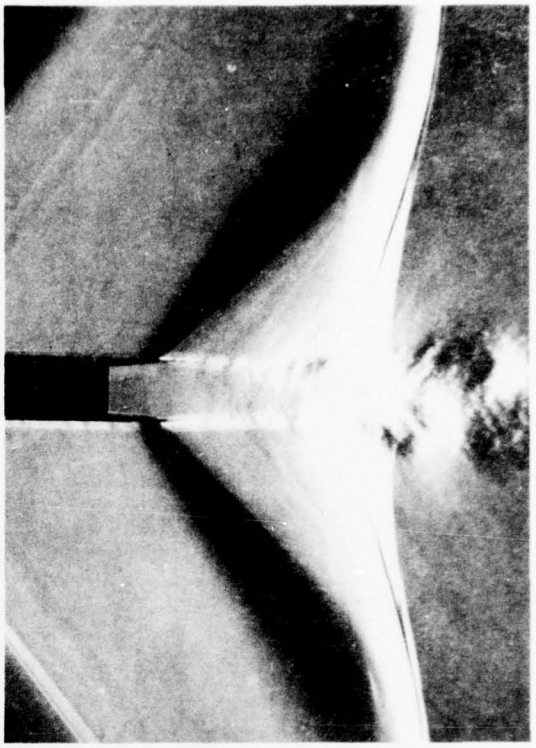

$C_q = 0.027 \quad C_{p_b} = -0.500$

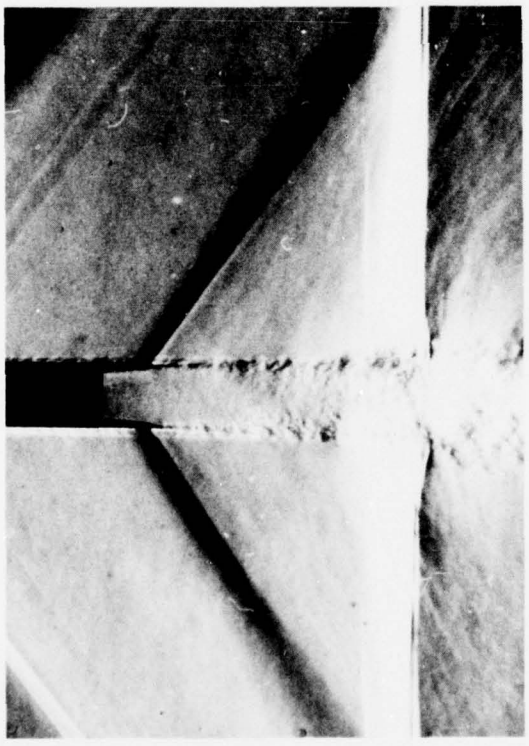

$C_q = 0.048 \quad C_{p_b} = -0.368$

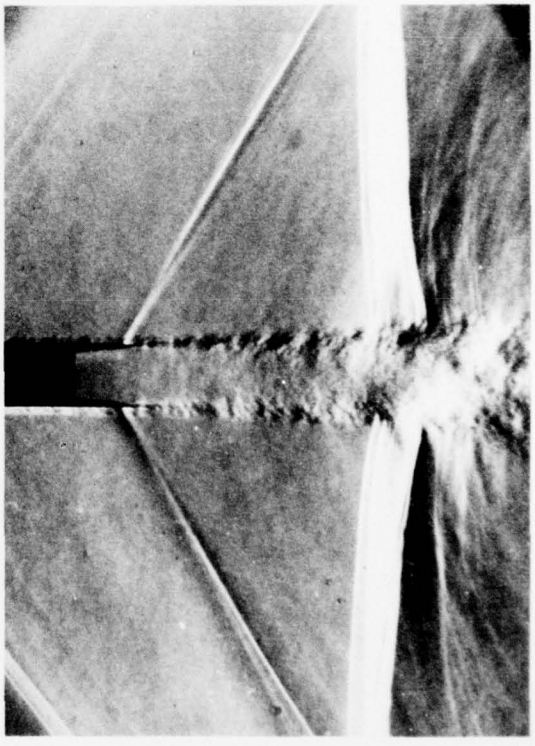

$C_q = 0.056 \quad C_{p_b} = -0.327$

FIG. 14. SCHLIEREN PHOTOGRAPHS OF BASE FLOW $M_o = 0.95$

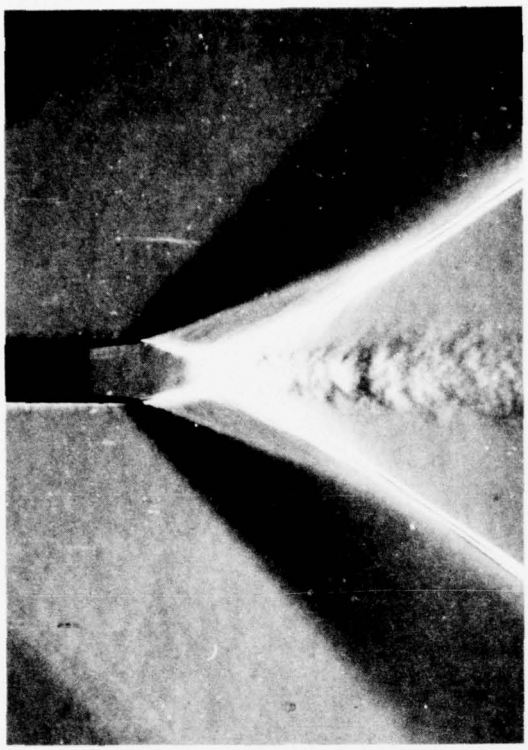

$C_q = 0$ $C_{p_b} = -0.432$

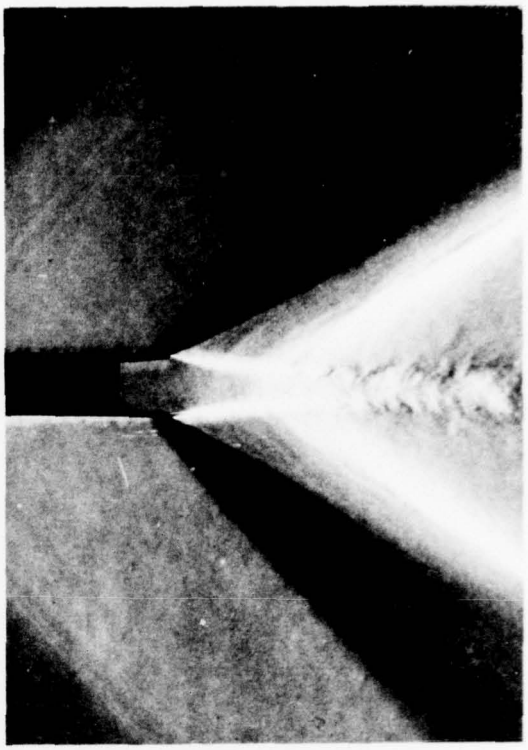

$C_q = 0.023$ $C_{p_b} = -0.323$

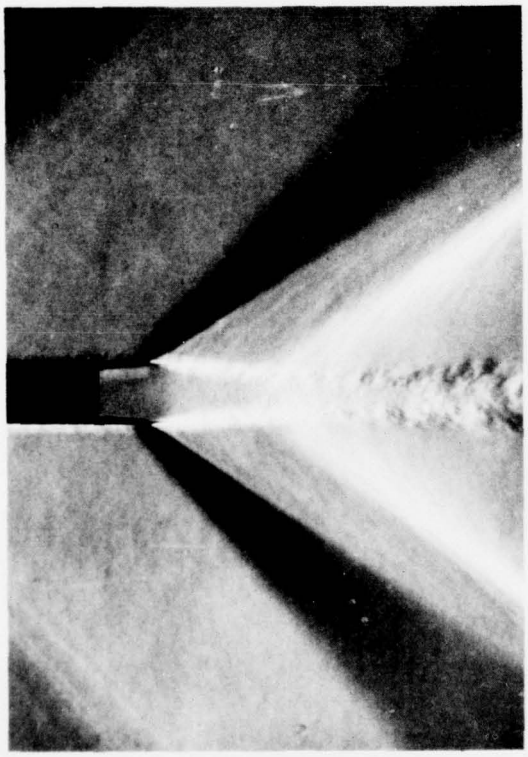

$C_q = 0.04$ $C_{p_b} = -0.263$

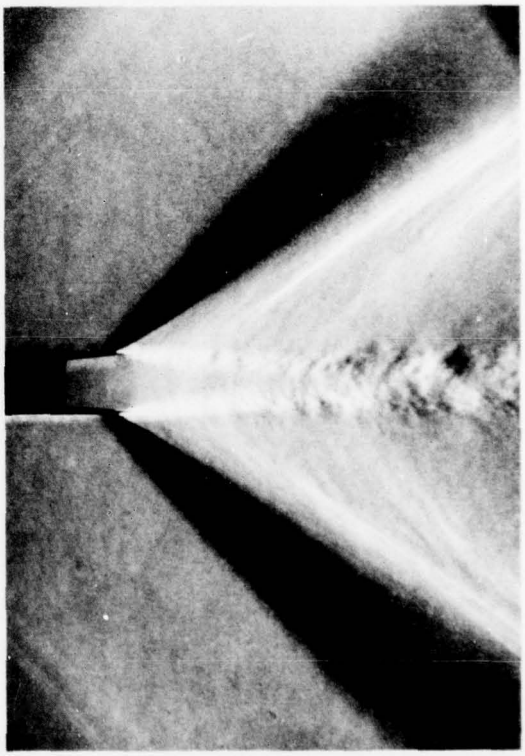

$C_q = 0.05$ $C_{p_b} = -0.242$

FIG. 15. SCHLIEREN PHOTOGRAPHS OF BASE FLOW $M_o = 1.30$

Curve	———	—·—·—	- - - -
Data Source	Present Tests	Bearman Ref. 10	Wood Ref. 9
M_o	0.5	0.03-0.08	0.1
Re	$5.8\text{-}10\times10^4$	$1.3\text{-}4.1\times10^4$	8×10^4
$\frac{h}{\theta}$	70	60	?
Aspect ratio	4.37	4.67	0.7
$\frac{\text{Bleed area}}{\text{Base area}}$	0.93	0.93 with porous filler	0.93

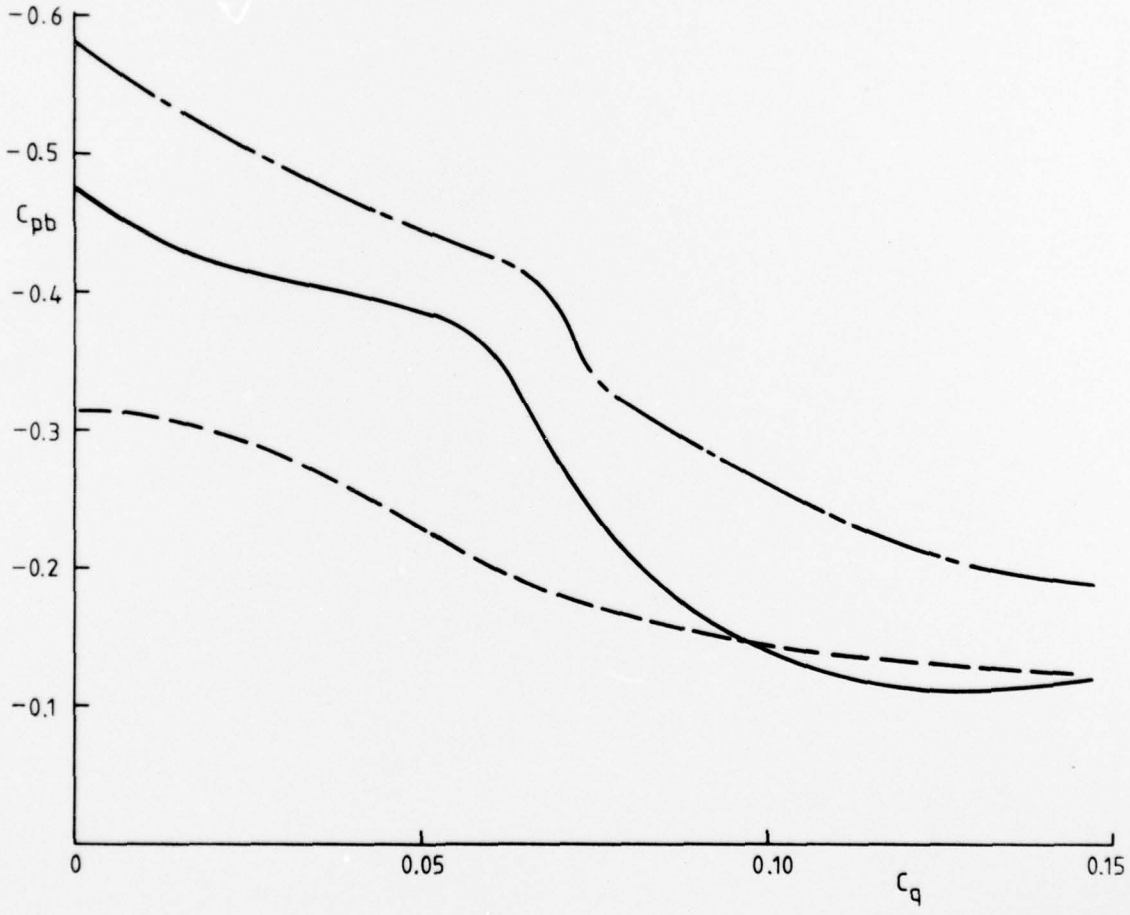

FIG. 16. COMPARISON WITH OTHER LOW SPEED RESULTS

Curve	———	— - —	- - - -
Data Source	Present Tests	Sirex Ref. 13	Ginoux Ref. 14
$\frac{h}{\theta}$	70	100	74

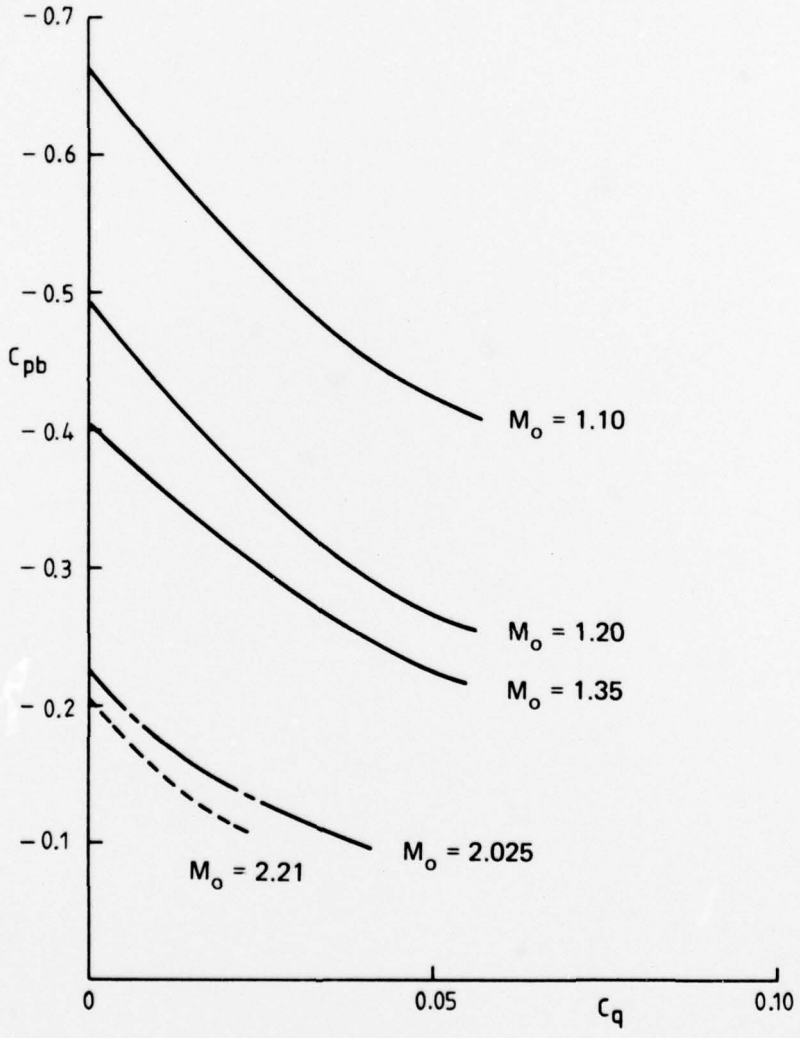

FIG. 17. COMPARISON WITH OTHER SUPERSONIC RESULTS

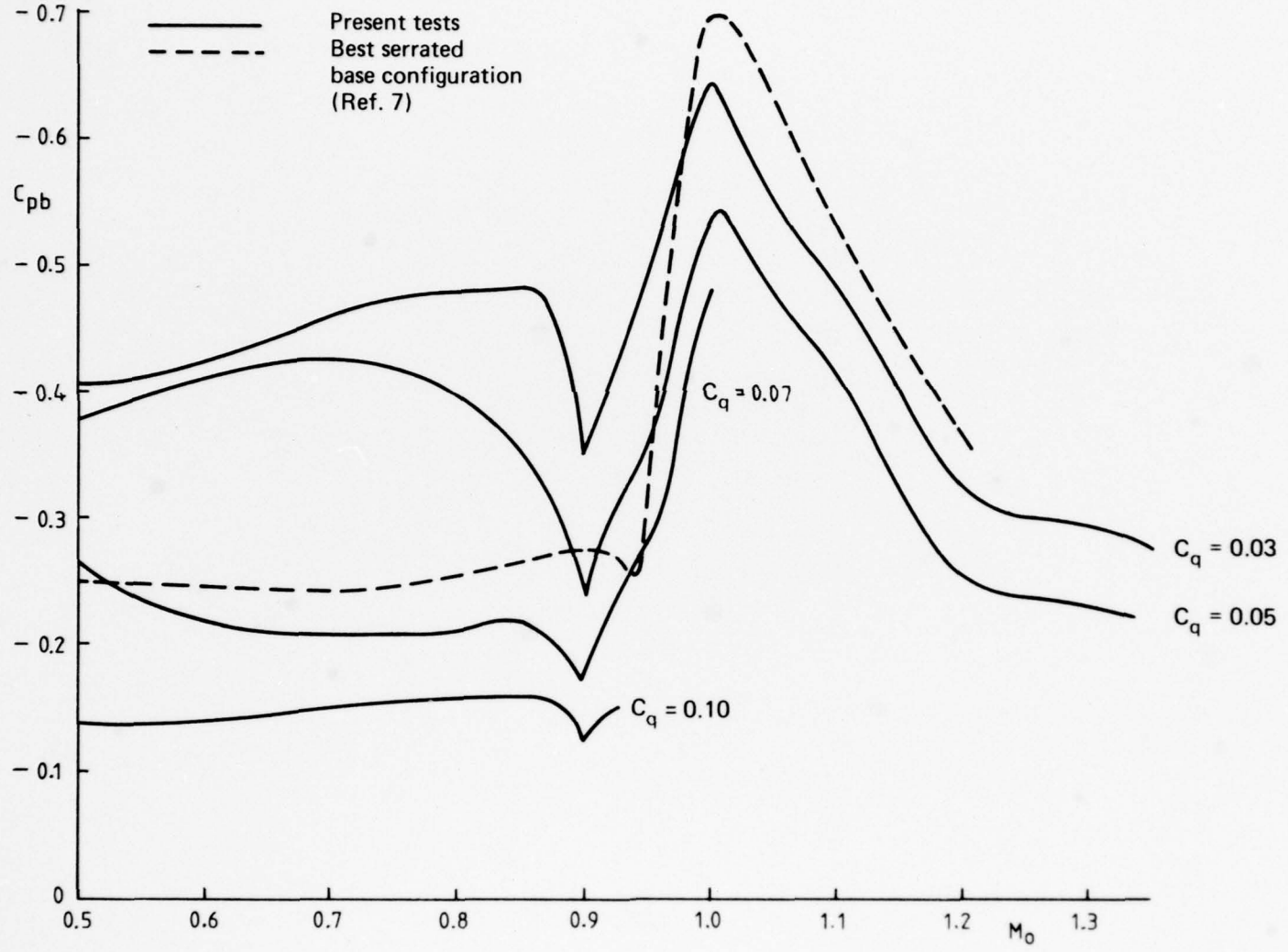

FIG. 18. COMPARISON WITH BEST SERRATED BASE CONFIGURATION

DOCUMENT CONTROL DATA SHEET

Security classification of this page: Unclassified

1. Document Numbers
   (a) AR Number:
   AR-001-321
   (b) Document Series and Number:
   Aerodynamics Note 381
   (c) Report Number:
   ARL-Aero-Note 381

2. Security Classification
   (a) Complete document:
   Unclassified
   (b) Title in isolation:
   Unclassified
   (c) Summary in isolation:
   Unclassified

3. Title: THE EFFECT OF BLEED ON TWO-DIMENSIONAL BASE FLOW AT SUBSONIC, TRANSONIC AND LOW SUPERSONIC SPEEDS.

4. Personal Author(s):
   N. Pollock

5. Document Date:
   November, 1978

6. Type of Report and Period Covered:

7. Corporate Author(s):
   Aeronautical Research Laboratories

8. Reference Numbers
   (a) Task:
   DST 76/102
   (b) Sponsoring Agency:

9. Cost Code:
   54 7710

10. Imprint
    Aeronautical Research Laboratories,
    Melbourne

11. Computer Program(s)
    (Title(s) and language(s)):

12. Release Limitations (of the document)
    Approved for public release

12-0. Overseas:	No.		P.R.	1	A		B		C		D		E	

13. Announcement Limitations (of the information on this page):
    No Limitation

14. Descriptors:

Base flow	Transonic flow	0103
Base bleed	Wind tunnel tests	2004
Airfoils	Trailing edges	

15. Cosati Codes:

16.

ABSTRACT

Measurements of the effect of bleed on the base pressure acting on a two dimensional blunt training edge aerofoil are reported and schlieren photographs of the base flow are presented. The tests covered a Mach number range of 0·5 to 1·35 at a base height Reynolds number of approximately 9×10^4 with turbulent approach boundary layers.

The results indicate that small bleed quantities can produce considerably greater base drag reductions at transonic speeds than at subsonic or supersonic speeds. A bleed mass flow coefficient of 0·07 produces a lower base drag than the best practical non-bleed blunt trailing edge geometry through the entire test Mach number range.

DISTRIBUTION

AUSTRALIA

DEPARTMENT OF DEFENCE

Gas & Fuel Corporation of Victoria (Research Director) 47
S.E.C. Herman Research Laboratory (Librarian) Victoria 48
Commonwealth Aircraft Corporation (Manager of Engineering) 49
Hawker de Havilland Pty Ltd (Librarian) Bankstown 50
Hawker de Havilland Pty Ltd (Manager) Lidcombe 51

UNIVERSITIES AND COLLEGES

Adelaide	Library	52
	Professor of Mechanical Engineering	53
Australian National	Library	54
Flinders	Library	55
James Cook	Library	56
La Trobe	Library	57
Melbourne	Engineering Library	58
Monash	Library	59
Newcastle	Library	60
New England	Library	61
New South Wales	Physical Sciences Library	62
	Professor R. A. A. Bryant, Mechanical and Industrial Eng.	63
Queensland	Library	64
	Professor A. F. Pillow, Applied Mathematics	65
Sydney	Professor G. A. Bird, Aeronautical Engineering	66
	Professor J. W. Roderick, Mechanical Engineering	67
	Professor R. I. Tanner, Mechanical Engineering	68
Tasmania	Engineering Library	69
	Professor A. R. Oliver, Civil and Mechanical Engineering	70
Western Australia	Library	71
	Professor Allen-Williams, Mechanical Engineering	72
RMIT	Library	73
	Mr. H. Millicer, Aeronautical Engineering	74
	Mr. Pugh, Mechanical Engineering	75

CANADA

NRC, National Aeronautics Establishment, Library 76
NRC, Div. of Mech. Eng., Gas Dynamics Laboratory (Mr. R. A. Tyler) 77

UNIVERSITIES

McGill	Library	78
Toronto	Institute for Aerospace Studies	79

FRANCE

AGARD, Library 80
ONERA, Library 81
Service de Documentation, Technique de l'Aeronautique 82

GERMANY

ZLDI 83
DFVLR-AVA Gottingen (Dr. M. Tanner) 84

INDIA

Defence Ministry, Aero Development Establishment, Library 85
Hindustan Aeronautics Ltd, Library 86
Indian Institute of Science, Library 87
Indian Institute of Technology, Library 88
National Aeronautical Laboratory (Director) 89

ISRAEL

Technion—Israel Institute of Technology (Professor J. Singer) 90

Cambridge	Library, Engineering Department	129
	Professor G. K. Batchelor	130
	Professor M. J. Lighthill	131
Liverpool	Professor J. H. Preston, Fluid Mechanics Department	132
London	Professor A. D. Young, Queens College	133
Nottingham	Library	134
Southampton	Library	135
Strathclyde	Library	136
Cranfield Institute	Professor Lefebvre	137
of Technology	Library	138
Imperial College	The Head	139
	Professor of Mechanical Engineering	140

UNITED STATES OF AMERICA

NASA Scientific and Technical Information Facility	141
Sandia Group (Research Organisation)	142
American Institute of Aeronautics and Astronautics	143
Applied Mechanics Reviews	144
The John Crerar Library	145
Boeing Co. Industrial Production Division	146
Lockheed Aircraft Co. (Director)	147
McDonnell Douglas Corporation (Director)	148
United Technologies Corporation, Fluid Dynamics Laboratories	149
Battelle Memorial Institute, Library	150
Calspan Corporation	151

UNIVERSITIES AND COLLEGES

California	Dr. M. Holt, Department of Aerosciences	152
Florida	Mark H. Clarkson, Department of Aeronautical Engineering	153
Harvard	Professor A. F. Carrier, Div. of Eng. and Applied Math.	154
	Professor H. M. Emmons	155
	Dr. S. Goldstein, Div. of Eng. and Applied Physics	156
Illinois	Professor N. M. Newmark, Talbot Laboratories	157
Johns Hopkins	Professor S. Corrsin, Department of Mech. Eng.	158
Princeton	Professor G. L. Mellor	159
Stanford	Library, Department of Aeronautics	160
Wisconsin	Memorial Library, Serials Department	161
Brooklyn Institute of Polytechnology	Library, Polytech Aeronautical Laboratories	162
California Institute of Technology	Library, Guggenheim Aeronautical Laboratories	163
Massachusetts Institute of Technology	Library	164

Spares 165–174